The Pennsylvania State University

The Graduate School

Department of Mathematics

DYNAMICS OF LOCAL MAP FOR A DISCRETE BRUSSELATOR MODEL

A Thesis in

Mathematics

by

Hunseok Kang

Submitted in Partial Fulfillment
of the Requirements
for the Degree of

Doctor of Philosophy

August 2007

The thesis of Hunseok Kang was reviewed and approved* by the following:

Yakov Pesin
Distinguished Professor of Mathematics
Thesis Advisor
Chair of Committee

Leonid Berlyand
Professor of Mathematics

Mark Levi
Professor of Mathematics

Mark Strikman
Professor of Mathematics

John Roe
Professor of Mathematics
Chair of the Mathematics Department

*Signatures are on file in the Graduate School.

Abstract

The goal of the thesis is to describe the dynamics of the local map of coupled map lattice(CML) – the discrete Brusselator model. Following Kaneko I view CMLs as phenomenological models of the medium (which is assumed to be homogeneous and unbounded) and I present the dynamical system approach to the analysis of the global behavior of solutions of CML developed in works of V. Afraimovich, M. Brin, D. Orendovici, and Y. Pesin. This analysis is aimed at establishing spatio-temporal chaos associated with the set of traveling wave solutions of CML and describing the dynamics of the evolution operator on this set. The main results claim that the dynamics of the evolution operator on the set of traveling wave solutions is completely determined by the dynamics of the local map thus making the study of the latter as the primary goal of my research. In the case of the Brusselator model, the dynamics of the corresponding local maps is quite complicated, has many interesting properties and displays chaotic behaviors. The model depends on a number of parameters and the dynamics of the corresponding local map varies substantially when these parameters vary. In particular, the local map associated to the Brusselator model has the following properties: (1) it has an open domain of trajectories that escape to infinity; (2) it possesses the Julia set, i.e., an invariant domain that consists of bounded trajectories; (3) it has eventually trapping regions; (4) it has visiting regions; and (5) strange attractors inside the eventually trapping regions. Finally, I carried out the numerical study of strange attractors as well as various aspects of chaotic behaviors for this model.

Contents

Acknowledgements

First of all, I would like to express my deepest sense of gratitude to my advisor Professor Yakov Pesin for his patient guidance, encouragement and excellent advice throughout this study. I deeply feel indebted to my advisor all the time.

I would also like to express my gratitude to the members of my doctoral committee for their inspirations and generous assistance during this time.

Finally, I take this opportunity to express my profound gratitude to my beloved parent, parent in law, my wife and son for their moral support and patience during my study in the Pennsylvania State University.

Chapter 1

Introduction

In this chapter, we introduce a special class of infinite-dimensional dynamical systems, which is called *Coupled Map Lattices*. Then a review of the coupled map lattices is given, as well as a description of recent results relevant to this thesis. Finally, the results of this thesis are given.

1.1 Coupled Map Lattice

Coupled map lattices (CML) form a special class of infinite-dimensional dynamical systems. They are described by the equation of the form

$$u_{\bar{j}}(n+1) = f(u_{\bar{j}}(n)) + \epsilon g_{\bar{j}}(\{u_{\bar{i}}(n)\}_{|\bar{i}-\bar{j}|\leq s}). \tag{1.1.1}$$

Here $n \in \mathbb{Z}$ is the discrete time coordinate, $\bar{j} = (j_k)$, $k = 1, ..., p$, the discrete space coordinate, and $u(\bar{j}, n) = u_{\bar{j}}(n)$ is a characteristic of the medium (for example, its density, or distribution of the temperature, etc.). Furthermore, $f : \mathbb{R}^d \to \mathbb{R}^d$ and $g_{\bar{j}} : (\mathbb{R}^d)^{(2s+1)} \to \mathbb{R}^d$ are smooth functions; f is called the *local map* and g the *interaction* of size s (where s can be infinite). Finally, ϵ is a parameter which is assumed to be sufficiently small.

Natural sources of CML are discrete versions of partial differential equations of evolution type. They arise while modeling partial differential equations by a computer. In general, no information on the global behavior of solutions of a partial differential equation can be derived from the study of its discrete versions even when steps of discretization are small. However, we believe that some methods of studying spatio-temporal chaos in CML, described in this thesis, can be applied (perhaps with some modifications) to partial differential equations.

In [Kan93], Kaneko developed a new point of view on CML as phenomenological models which can be used to describe the behavior of an unbounded medium with high level of energy pumping (corresponding to large Reynolds numbers; cf also [Bun95]). In this case one can observe particle-like localized structures, i.e., distinct spatial structures obeying individual dynamics and interacting with nearest neighbors. Moreover, if the medium is spatio-homogeneous the individual dynamics are identical. Thus, the behavior of the medium obeys Equation (1.1.1) (with the local map f representing the individual dynamics). This is the way to build a phenomenological lattice model. The discovery by Kaneko has drown attention of many physicists and mathematicians to CML and exposed a great interest to this area.

The dynamical system approach to the study of CML was originated by Bunimovich and Sinai (see [BS88]) and since that has become a core technique in the theory. See, for example, [AGN94], [BK96], [JP98], and [KK92]. The main achievement of this approach is the description of the global behavior of solutions of Equation (1.1.1) for a broad class of local maps exhibiting greater or lesser hyperbolicity.

Traveling wave solutions were first studied as a class of solutions of the CML by Afraimovich and Pesin in [AP93]. They studied the stability of motion in the form of traveling waves in the CMLs and showed that under certain conditions on the local maps the set of traveling wave solutions forms a finite-dimensional submanifold in infinite-dimensional phase space endowed with a special norm with weight. Finally, they concluded that the dynamics of the evolution operator on the set of traveling wave solutions is completely determined by the traveling wave map, and the traveling wave map and the local map share many dynamical properties under the assumption that the interaction is sufficiently small.

In [OP99], Orendovici and Pesin established finite-dimensional spatial-temporal chaos associated with traveling wave solutions of the CML. Also they presented some interesting examples of CMLs describing their hyperbolic, topological, and ergodic properties.

The main goal of this thesis is to explore the dynamics of the nonlinear local map of the CML which are obtained by discretizing the Brusselator model. We studied the dynamical properties of these local maps and checked if these properties can be related to the dynamics of the evolution operators restricted to traveling wave solutions of the CML.

1.2 Discretizations of Partial Differential Equations

There are many partial differential equations of evolution type whose discrete versions are coupled map lattices of the form (1.1.1). Among them we consider some nonlinear reaction-diffusion systems, which corresponds to nonlinear local maps.

1.2.1 Nonlinear reaction-diffusion equation

Reaction-diffusion equations are members of partial differential equations of evolution type. It is described by

$$u_t = h(u) + \mathcal{A}\kappa\Delta u, \tag{1.2.1}$$

where $x \in \mathbb{R}^p$ is the space coordinate, $t \in \mathbb{R}$ is time, $u = u(x,t)$ is a function with values in $\mathbb{R}^d$, $\mathcal{A}$ is the $d \times d$ coupling matrix, and κ is the diffusion coefficient.

Equation (1.2.1) describes a large variety of phenomena in different fields. For example, heat conductivity in physics, chemical diffusion processes in chemistry, kinetics of enzyme in biology, propagation of voltage impulse through a nerve axon in neurophysiology (see [HH52] and [KPP37] for more applications).

1.2.2 Discretizations

One can obtain discrete versions of the above partial differential equations replacing derivatives by appropriate differences. This is usually the way the equation is studied by a computer.

For the derivative in time we use

$$\frac{\partial u(x,t)}{\partial t} \to \frac{u(x,t+\Delta t) - u(x,t)}{\Delta t}. \tag{1.2.2}$$

And for the space derivative we use

$$\begin{aligned} \frac{\partial u(x,t)}{\partial x} &\to \frac{u(x+\Delta x,t) - u(x,t)}{\Delta x}, \\ \frac{\partial^2 u(x,t)}{\partial x^2} &\to \frac{u(x+\Delta x,t) - 2u(x,t) + u(x-\Delta x,t)}{(\Delta x)^2}. \end{aligned} \tag{1.2.3}$$

A number of models which appear in physics, biology, chemistry, etc are described by the reaction-diffusion equations (See [OP99] and [PY04].). In this thesis, we will deal with a few models among them, which are described

by two-dimensional reaction-diffusion equations: The FitzHugh's model of the propagation of voltage impulse through a nerve axon, Brusselator model for the Belousov-Zhabotinsky reaction, and Turing's continuous model of morphogenesis.

1.3 Traveling Wave Solution

In [OP99], the authors discussed the mechanism for appearance of finite dimensional spatial and/or temporal chaos associated with various special classes of solutions including steady-state, spatio-homogeneous, and traveling wave solutions. Among these classes of solutions, we focus on the class of traveling wave solutions.

CMLs have a class of solutions known as traveling wave solutions. Traveling wave solutions running with a given velocity form a finite-dimensional smooth submanifold in the infinity-dimensional phase space which is invariant under both time and space translations.

1.3.1 Evolution Operator on Phase Space

Consider the direct product of finite-dimensional Euclidean spaces $\mathcal{R} = \bigotimes_{\mathbb{Z}^p} \mathbb{R}^d = (\mathbb{R}^d)^{\mathbb{Z}^p}$. Given $q_1 = (q_{1,i})$, $q_2 = (q_{2,i})$ with $q_{1,i} > 1$, $q_{2,i} > 1$, $i = 1, ..., p$ and $u = (u_{\bar{j}}) \in \mathcal{R}$, $\bar{j} \in \mathbb{Z}^p$, we set

$$\|u\|_{q_1,q_2} = \sum_{j_1} \cdots \sum_{j_p} \frac{|u(\bar{j})|}{q(j_1) \cdots q(j_p)}, \tag{1.3.1}$$

where $\bar{j} = (j_i)$ and $q(j_i) = (q_{1,i})^{j_i}$ if $j_i \geq 0$ and $q(j_i) = (q_{2,i})^{-j_i}$ if $j_i < 0$. This norm $\|\cdot\|_{\cdot,\cdot}$ is called **norm with weights**.

The CMLs (1.1.1) can be described as the infinite-dimensional dynamical system $(\mathcal{M}_{q_1,q_2}, \Phi)$ with the underlying phase space

$$\mathcal{M}_{q_1,q_2} = \{u = (u_{\bar{j}}) : \|u\|_{q_1,q_2} < \infty\} \tag{1.3.2}$$

and the non-linear evolution operator $\Phi = \Phi_\epsilon$

$$(\Phi u)_{\bar{j}}(n) = f(u_{\bar{j}}(n)) + \epsilon g_{\bar{j}}(\{u_{\bar{i}}(n)\}_{|\bar{i}-\bar{j}|\leq s}).$$

Then the dynamical system $(\mathcal{M}_{q_1,q_2}, \Phi)$ corresponds to solutions of the CML which satisfy the initial condition $(u_{\bar{j}}(0)) \in \mathcal{M}_{q_1,q_2}$ and the boundary condition $\|u\|_{q_1,q_2} < \infty$, i.e., the solution may grow at infinity with exponential rate.

We observe that $\mathcal{M}_{q_1,q_2}$ is a Banach space with respect to the metric $\|\cdot\|_{q_1,q_2}$. Moreover, the operator Φ has a special form $\Phi = F + \epsilon G$ where $F = \bigotimes_{\mathbb{Z}^p} f$ and $G = (g_{\bar{j}})_{\bar{j}\in\mathbb{Z}^p}$. If ϵ is sufficiently small, Φ can be viewed as a small perturbation of F.

In [AP93] Afraimovich and Pesin made the following two assumptions **A1** and **A2** on the local map f and the interaction g in order for the space $(\mathcal{M}_{q_1,q_2}, \Phi)$ to be a well-defined dynamical system.

A1. There exists $K > 0$ such that for $l = 1, 2$:

$$\sup_{x\in\mathbb{R}^d} \|D^l f_x\| \le K,$$

$$\sup_{1\le i\le 2s+1} \sup_{x\in(\mathbb{R}^d)^{2s+1}} \left\| \frac{\partial^l g}{\partial x_i^l} \right\| \le K;$$

A2. For any $x = (x_i) \in (\mathbb{R}^d)^{2s+1}$,

$$\det\left(\frac{\partial g(x)}{\partial x_1}\right) \neq 0,$$

$$\sup_{x\in(\mathbb{R}^d)^{2s+1}} \det\left(\frac{\partial g(x)}{\partial x_1}\right)^{-1} < \infty.$$

Note that, in these assumptions **A1** and **A2**, f and g are not necessarily supposed to be bounded but their first and second derivatives are required to be bounded.

The space $\mathcal{M}_{q_1,q_2}$ admits **spatial translations (or shift)** $S^{\bar{k}} : \mathcal{M}_{q_1,q_2} \to \mathcal{M}_{q_1,q_2}$ given by

$$S^{\bar{k}}(u)_{\bar{i}} = u_{\bar{i}+\bar{k}}, \tag{1.3.3}$$

where $\bar{i} = (i_j)$, $\bar{k} = (k_j) \in \mathbb{Z}^p$. We now assume that the following condition holds:

A3. the maps Φ^l and $S^{\bar{k}}$ commute for any $l \in \mathbb{Z}$ and $\bar{k} \in \mathbb{Z}^p$.

Note that if the interaction $g_{\bar{j}}$ does not depend on j the assumption **A3** holds. This is the case when the lattice system is obtained as a discretization of a partial differential equation.

Under the assumption **A3**, the map $\{(\Phi^l, S^{\bar{k}}) : l \in \mathbb{Z}, \bar{k} \in \mathbb{Z}^p\}$ generates an action of the $\mathbb{Z}^{p+1}$-lattice on $\mathcal{M}_{q_1,q_2}$.

1.3.2 Types of Chaotic Behavior in Lattice Systems

In [PS91], Pesin and Sinai discussed the following types of chaotic behavior in lattice systems corresponding to actions of temporal and/or spatial translations. A lattice dynamical system is said to display:

1. **temporal chaos** if there exists a measure μ invariant under the $\mathbb{Z}^1$-action $\{\Phi^l\}$ which is mixing;

2. **spatial chaos** if there exists a measure μ invariant under the $\mathbb{Z}^p$-action $\{S^{\bar{k}}\}$ which is mixing;

3. **spatio-temporal chaos** if there exists a measure μ invariant under the $\mathbb{Z}^{p+1}$-action $\{\Phi^l, S^{\bar{k}}\}$ which is mixing;

In many cases the chaotic behavior of lattice systems is essentially finite-dimensional. This means that there exists a finite-dimensional (often smooth) submanifold in the infinite-dimensional phase space which is invariant with respect to time translations or space translations or both and which supports an invariant mixing measure. Such submanifolds are usually associated with special classes of solutions.

It may also happen that such a submanifold is *stable* in the infinite-dimensional phase space, i.e., solutions which start in a small neighborhood of this submanifold approach it with time.

In this case chaotic behavior is persistent and thus is *physically observable*. Otherwise, chaotic behavior occurs on a *tiny* finite-dimensional submanifold and is *invisible*. In some cases the invariant submanifold is stable in a weaker sense: it possesses an infinite-dimensional separatrix which is everywhere dense in the phase space. In this case the chaotic behavior should also be considered as physically observable. However, it is essentially unstable (with respect to small perturbations of initial data) and hence, is significantly more difficult to study.

1.3.3 Traveling Wave Solutions of Coupled Map Lattices

In [AP93] Afraimovich and Pesin studied finite-dimensional spatial-temporal chaos in traveling waves for some lattice system. They first introduced another class of solutions known as traveling wave solutions to the solution of CMLs. In [OP99], Orendovici and Pesin showed that traveling

wave solutions form a finite-dimensional smooth submanifold in the infinite-dimensional phase space which is invariant under both time and space translations. Also, they observed finite-dimensional spatial-temporal chaos associated with traveling waves.

In this thesis, I describe the traveling wave solutions in the case that the space translation is one-dimensional, i.e., $p = 1$ in (1.3.3), for simplicity. Let m and l be integers. A **traveling wave solution** of Equation (1.1.1) is a solution of the form:

$$u_j(n) = \psi(lj + mn), \tag{1.3.4}$$

where $\psi : \mathbb{Z} \to \mathbb{R}^d$ is a function. The numbers m and l determine the velocity of the wave. When $p = 1$, the norm (1.3.1) in the phase space $\mathcal{M}_{q_1,q_2}$ (1.3.2) is determined by two numbers $q_1 > 1$, $q_2 > 1$ in the following way

$$\|u\|_{q_1,q_2} = \sum_{j<0} \frac{|u_j|}{q_1^{-j}} + \sum_{j\geq 0} \frac{|u_j|}{q_2^{j}},$$

Assume that m and l are relatively prime and $m > ls+1$ so that the velocity of the wave is large. Also assume that the interaction $g_j(x_1, ..., x_{2s+1})$ in Equation (1.1.1) does not depend on j, i.e., $g_j = g$.

Then the function ψ in (1.3.4) must satisfy the following **traveling wave equation**:

$$\psi(k) = f(\psi(k - m)) + \epsilon g(\{\psi(k - m + li)\}_{|i|\leq s}), \tag{1.3.5}$$

where $k = lj + mn + m$ is called the traveling coordinate.

Denote by $\Psi = \Psi(\epsilon, q_1, q_2, m, l, s)$ the set of solutions of the traveling wave equation which is a subset in $(\mathbb{R}^d)^{\mathbb{Z}}$. In view of our assumptions on m and l, Equation (1.3.5) is an equation with delay argument (i.e., $k-m+ls \leq k-1 < k$). Therefore, a traveling wave is uniquely determined by the values:

$$x_p = \psi(-m - ls + p + 1) \quad \text{for } p = 1, ..., ls + m.$$

The dynamics on the set Ψ of traveling waves is given by the **shift map** Q_ϵ defined by $Q_\epsilon(\psi)(k) = \psi(k + 1)$. In [AP93], it is demonstrated that the dynamics on the set Ψ of traveling waves is finite-dimensional and is governed by the traveling wave map $F_\epsilon : (\mathbb{R}^d)^{ls+m} \to (\mathbb{R}^d)^{ls+m}$ given by

$$F_\epsilon(x_1, ..., x_{ls+m}) = (x_2, ..., x_{ls+m}, f(x_{ls+1}) + \epsilon g(x_{p(i)})_{i=-s}^{s}), \tag{1.3.6}$$

where $p(i) = l(s + i) + 1$. One of the main results is as follows:

Theorem 1.3.1. There exist two constants $q_1^{(0)} > 1$, $q_2^{(0)} > 1$ such that for any $q_1 > q_1^{(0)}$, $q_2 > q_2^{(0)}$, the traveling wave map F_ϵ^m are smoothly conjugate to the evolution operator Φ_ϵ; in other words, there exists a smooth embedding χ of $(\mathbb{R}^d)^{ls+m}$ into $\mathcal{M}_{q_1,q_2}$ such that the following diagram is commutative:

$$\begin{array}{ccc} (\mathbb{R}^d)^{ls+m} & \xrightarrow{\chi} & \mathcal{A}_{q_1,q_2} \subset \mathcal{M}_{q_1,q_2} \\ {\scriptstyle F_\epsilon^m}\downarrow & & \downarrow{\scriptstyle \Phi_\epsilon} \\ (\mathbb{R}^d)^{ls+m} & \xrightarrow{\chi} & \mathcal{A}_{q_1,q_2} \subset \mathcal{M}_{q_1,q_2} \end{array}$$

where $\mathcal{A}_{q_1,q_2} = \chi\left((\mathbb{R}^d)^{ls+m}\right)$ is a smooth submanifold in $\mathcal{M}_{q_1,q_2}$ of dimension $d(ls+m)$.

The way to construct the map χ and the submanifold $\mathcal{A}_{q_1,q_2}$ in Theorem 1.3.1 above is explicitly described in [AP93]. Therefore, the dynamics of the evolution operator on the set of traveling wave solutions is conjugated to the dynamics of the traveling wave map F_ϵ.

1.4 Dynamics of the Traveling Wave Map

In Section 1.3, we understood that the dynamics of the evolution operator Φ_ϵ on the set of traveling wave solutions running with a given velocity is completely determined by the traveling wave map F_ϵ. In this section, we describe hyperbolic properties of the traveling wave map (1.3.6), i.e., properties which characterize instability of trajectories, and also, we discuss how to relate it to the local map, which is hyperbolic in a strong sense as well as in a weak sense.

1.4.1 The Case of Hyperbolic Local Map

Our goal here is to illustrate that for sufficiently small interactions these properties are dominated by the hyperbolic behavior of the local map f. In particular, we show that if the local map is hyperbolic in a strong sense (i.e., it possesses a hyperbolic set; every trajectory in this set is highly unstable) then so are the traveling wave map and the restrictions of space and time translations to the submanifold of traveling wave solutions. This implies that the CML displays chaotic behavior of the highest degree, i.e., there exists a measure invariant under space and time translations which is supported on the set of traveling wave solutions and has ergodic properties of higher order.

Consider a generalization of traveling wave map, $F_\epsilon : (\mathbb{R}^d)^m \to (\mathbb{R}^d)^m$, given by

$$F_\epsilon(x_1, ..., x_k, ..., x_n) = (x_2, ..., x_{k+1}, ..., f(x_k) + \epsilon g(x_i)_{i=1}^n) \,. \tag{1.4.1}$$

We assume that $f : \mathbb{R}^d \to \mathbb{R}^d$ and $g : (\mathbb{R}^d)^n \to \mathbb{R}^d$ satisfy conditions **A1** and **A2** so that F_ϵ is a local diffeomorphism.

We consider the case when the local map f possesses a locally maximal hyperbolic set Λ. A compact invariant set Λ is called **hyperbolic** if for every $x \in \Lambda$ there exists a splitting of the tangent space T_xM at x into two subspaces $E^s(x)$ and $E^u(x)$, $TM_\Lambda = E^s(x) \oplus E^u(x)$ such that:

1. the splitting is invariant under the differential df, i.e.,

$$df(E^s(x)) = E^s(f(x)), \quad df(E^u(x)) = E^u(f(x));$$

2. the subspaces $E^s(x)$ and $E^u(x)$ are respectively **stable** and **unstable** for the differential df, i.e.,

$$|df_x^n v| \le c\lambda^n |v|$$

for every $v \in E^s(x)$ and

$$|df_x^n v| \ge c^{-1}\lambda^{-n} |v|$$

for every $v \in E^u(x)$, where $c > 0$ and $0 < \lambda < 1$ are constants independent of x and v.

A hyperbolic set Λ is said to be **locally maximal** if there exists an open neighborhood V of Λ such that

$$\Lambda = \bigcap_{n=-\infty}^{\infty} f^n(V).$$

In [AP93], the authors studied hyperbolic properties of the map F_ϵ for sufficiently small ϵ using a modification of the classical perturbation theorem for hyperbolic sets. They have

Theorem 1.4.1. There exists $\epsilon_0 > 0$ such that for any $0 < \epsilon < \epsilon_0$ there is an invariant locally maximal hyperbolic set Λ_ϵ for F_ϵ in (1.4.1).

We also consider the traveling wave map F_ϵ. By Theorem 1.4.1, for sufficiently small ϵ there exists a locally maximal hyperbolic set Λ_ϵ for F_ϵ. Let μ be an invariant mixing measure on Λ_ϵ. In Theorem 1.3.1, using the map χ, we can push this measure on $\mathcal{A}_{q_1,q_2}$ (see the diagram in Theorem 1.3.1). Hence, we obtain the measure $\mu_{q_1,q_2} = \chi * \mu$.

Theorem 1.4.2 (see [AP93])**.** The measure μ_{q_1,q_2} is invariant under time and space translations and is mixing.

Therefore, the lattice dynamical system displays spatio-temporal chaos.

1.4.2 The Case of Local Map of Morse-Smale Type

We now consider the case when the local map f is a Morse-Smale diffeomorphism. Morse-Smale diffeomorphisms are hyperbolic in a weak sense: there exist finitely many hyperbolic periodic points which determine the behavior of all other orbits. These systems are not chaotic, in fact, the behavior of every single trajectory is well understood: all of them (except hyperbolic periodic points) move towards attracting periodic points as time increases and towards repelling periodic points as time decreasing. Our goal here is to show that for sufficiently small interactions the traveling wave map F_ϵ is also of Morse-Smale type and so are space and time translations restricted to the set of traveling wave solutions. Thus, the topological behavior of CML is completely understood and is not chaotic.

Let M be a smooth compact Riemannian manifold and $\mathcal{F} : M \to M$ a C^1-diffeomorphism. A point $x \in M$ is called **nonwandering** if for any neighborhood U of x there exists a positive integer n such that $\mathcal{F}^n(U) \cap U \neq \emptyset$. $\Omega(\mathcal{F})$ denotes the set of all nonwandering points of $\mathcal{F}$.

A point $x \in M$ is **periodic** if $\mathcal{F}^p(x) = x$ for some positive integer p. $\mathrm{Per}(\mathcal{F})$ denotes the set of all periodic points of $\mathcal{F}$.

An endomorphism $\mathcal{F}$ is called **Morse-Smale** if it satisfies the following properties:

1. $\Omega(\mathcal{F}) = \mathrm{Per}(\mathcal{F})$;
2. every periodic point is hyperbolic;
3. the local stable and global unstable manifolds of periodic points intersect transversally.

In [OP99], the authors used the standard stereograhpic projection and the compactification map $\tilde{f}$ of the local map f and gave some conditions on the compactification map $\tilde{f}$ and the interaction g to show that if the local map f is of Morse-Smale type, then so is the traveling wave map F_ϵ. More precisely, they proved

Theorem 1.4.3. There exists $\epsilon_0 > 0$ such that for any $0 < \epsilon < \epsilon_0$ the traveling wave map F_ϵ is a Morse-Smale endomorphism. Moreover, F_ϵ is a local diffeomorphism for $0 < \epsilon < \epsilon_0$.

1.4.3 Examples

We first deal with an example of hyperbolic local maps. In [OP99], Orendovici and Pesin proved that the local map corresponding to the FitzHugh-Nagumo equation possesses a locally maximal hyperbolic set. The FitzHugh-Nagumo model is described by a two-dimensional nonlinear reaction-diffusion equation

$$\begin{aligned} \frac{\partial u_1}{\partial t} &= -au_1(u_1-\theta)(u_1-1) - bu_2 + \kappa_1 \frac{\partial^2 u_1}{\partial x^2}, \\ \frac{\partial u_2}{\partial t} &= cu_1 - du_2 + \kappa_2 \frac{\partial^2 u_2}{\partial x^2}, \end{aligned}$$

where $\kappa_i \geq 0$ and a, b, c and d are all positive coefficients. See [HH52] for the details of this model. When discretized, the FitzHugh-Nagumo equation forms a CML and the corresponding local map is

$$f(u_1, u_2) = (u_1 - Au_1(u_1-\theta)(u_1-1) - \alpha u_2, \beta u_1 + \gamma u_2), \tag{1.4.2}$$

where $A = a\Delta > 0$ is a leading parameter, $\alpha = b\Delta t > 0$, $\beta = c\Delta t > 0$, $\gamma = (1 - d\Delta t) > 0$, $\theta \in (0,1)$ are parameters.

In [OP99], a **horseshoe-type** construction is developed to obtain an invariant subset Λ for the local map f under some conditions on the parameters, $\alpha > 0$, $\beta > 0$, $\gamma > 0$, and θ. They proved

Theorem 1.4.4. For all sufficiently large A there exists a rectangle $R = [\theta, 1] \times [r, s]$ such that the intersection $R \cap f(R)$ consists of two connected components R_1 and R_2.

Based on Theorem 1.4.4, one can now develop a "horseshoe-type construction" to obtain an invariant subset Λ for f. One can then use the standard "cone technique" to show that Λ is hyperbolic (see [OP99] for more details). More precisely, the following statement holds.

Theorem 1.4.5. The set

$$\Lambda = \bigcap_{n=-\infty}^{\infty} f^n(R)$$

is a locally maximal hyperbolic set for f.

An example of the local map of Morse-Smale type is the one corresponding to the Kolmogorov-Petrovskii-Piskunov (KPP) planar model of advance

of advantageous genes (See [KPP37].). This model is described by a one-dimensional reaction-diffusion equation

$$u_t(x,t) = \alpha u(1-u) + \kappa u(x,t),$$

where $\alpha > 0$ and κ is a positive diffusion constant. The local map corresponding to this equation above is

$$f(u) = u + \gamma u(1-u),$$

where $\gamma > 0$ is a parameter. In [OP99], the authors showed that

Theorem 1.4.6. There exists $\gamma_0 > 0$ such that for $0 < \gamma < \gamma_0$ the compactification map $\tilde{f}$ of f is of a Morse-Smale type and has four hyperbolic fixed points, and hence, so is f.

This implies that the traveling wave map F_ϵ is also of a Morse-Smale type. In addition, there are many one-dimensional local maps, for example, which are corresponding to the Huxley equation, the Swift-Hohenberg equation, and so on. See [PY04] for more examples. Also, the two-dimensional local map in (1.4.2), corresponding to the FitzHugh-Nagumo equation, is of a Morse-Smale type.

1.5 Dynamics of the Traveling Wave Map: the Case of Local Map with Strictly Forward-Invariant Sets

In this section, we consider the case when the local map f possesses a strictly forward-invariant region. For a given map ϕ on a metric space M, a set $U \subset M$ is said to be a *strictly forward-invariant set* provided that for each point $x \in U$, the forward orbit $\{\phi^n(x) : n > 0\}$ is contained in $\text{int}(U)$.

In this case, we may predict long-term behaviors of trajectories; where trajectories tend to head and how they behave after a sufficiently large number of iterations by the local map f. Our goal in this section is to show that for sufficiently small interactions the traveling wave map F_ϵ also possesses a strictly forward-invariant set and so does the evolution operator on the set of traveling wave solutions.

Theorem 1.5.1. Suppose that the local map f has a strictly forward-invariant region $\Omega \subset \mathbb{R}^d$ and the interaction g is bounded. Then there exists

$\epsilon_0 > 0$ such that for any $0 < \epsilon < \epsilon_0$ there exists a strictly forward-invariant region Θ

$$\Theta := \otimes_{i=1}^{ls+m}\Omega \subset (\mathbb{R}^d)^{ls+m}$$

for the traveling wave map F_ϵ.

Proof. Let $\partial(\Omega)$ and $\partial(f(\Omega))$ be the boundaries of Ω and $f(\Omega)$, respectively. Then $\partial(f(\Omega))$ lies strictly inside $\mathrm{int}(\Omega)$ and there exists $0 < \zeta_1 < \infty$ such that

$$\zeta_1 = \inf_{x\in\partial(\Omega),\ y\in\partial(f(\Omega))} \mathrm{dist}(x, y).$$

Since g is assumed to be bounded, there exists $0 < \zeta_2 < \infty$ such that

$$\zeta_2 = \sup_{z\in H} |g(z)| > 0,$$

where H is the direct product of Ω: $H = \otimes_{i=1}^{ls+m}\Omega$.

Set $\epsilon_0 = \zeta_1/(2\zeta_2)$. Then for any $0 < \epsilon < \epsilon_0$, $x \in \Omega$ and $z \in H$,

$$f(x) + \epsilon g(z)$$

is within ζ_1 from $f(x)$, and hence, it is within $\zeta_1/2$ from $\partial(\Omega)$. Iterating a point $(x_1, ..., x_{ls+m}) \in \Theta$, $(ls + m)$-times, by the traveling wave map F_ϵ yields

$$F_\epsilon^{ls+m}(x_1, ..., x_{ls+m}) = (\tilde{x}_1, ...\tilde{x}_{ls+m}),$$

where $\tilde{x}_k = f(y_k) + \epsilon g(z_k)$ for some $y_k \in \Omega$ and $z_k \in H$ for $k = 1, ..., ls + m$. Then each $\tilde{x}_k$ is within $\zeta_1/2$ from $f(y_k)$ so that $\tilde{x}_k \in \mathrm{int}(\Omega)$ and stays within $\zeta_1/2$ from $\partial(\Omega)$. Therefore, Θ is a strictly forward-invariant region under the map F_ϵ. □

One of the typical examples of strictly forward-invariant set is a trapping region. The trapping region is generally defined in the following sense: For a given map ϕ on a metric space M, a set $U \subset M$ is called a *trapping region* provided that there is $N > 0$ such that $\phi^N(\bar{U}) \subset \mathrm{int}(U)$ and U is bounded in M. So a trapping region can be regarded as a bounded strictly forward-invariant set.

In the case that the local map possesses a trapping region, for sufficiently small ϵ the traveling wave map F_ϵ also has a trapping region regardless of the boundedness of the interaction g. See [Kan07] for more detailed explanation and examples. We refer the definitions in this section from [Rob99].

As shown in Section 1.3 the dynamics of the local map determines the dynamics of the evolution operator for Equation (1.1.1). The latter is a

finite-dimensional subspace in the infinite-dimensional phase space of the system. In Section 2.3, we discuss another strictly forward-invariant region for a local map. Our results, in particular, provide a ground for existence of a Julia set for the evolution operator.

Chapter 2

Dynamics of a Discrete Brusselator Model, Part 1

In this chapter, we consider a discrete version of the Brusselator Model of the well-known Belousov-Zhabotinsky oscillatory reaction in chemistry. The original model is described by a reaction-diffusion equation, whose discrete version is a coupled map lattice. We study the dynamics of the local map, which is a smooth map of the plane. In this chapter, we focus on the behavior of unbounded trajectories. We discuss the set of trajectories that escape to infinity and describe how the unbounded trajectories escape to infinity. Also, we find the maximal region where every trajectory escapes to infinity. This can help us define the set of bounded trajectories – the Julia set of the system. Additionally, we study topological properties of this Julia set: closedness, unboundedness, and positivity of area of the Julia set.

2.1 Introduction

The Brusselator model is a famous model of chemical reactions with oscillations. It was proposed by Prigogine and Lefever in 1968 and the name was coined by Tyson (see [Tys76]). In the middle of the last century, Belousov and Zhabotinsky discovered chemical systems exhibiting oscillations. More precisely, they observed that cerium(III) and cerium(IV) were the cycling species: in a mix of potassium bromate, cerium(IV) sulfate, and citric acid in dilute sulfuric acid, the ratio of concentration of the $Ce(IV)$ and $Ce(III)$ ions oscillated. While for most chemical reaction a state of homogeneity and equilibrium is quickly reached, the Belousov-Zhabotinsky reaction is a remarkable chemical reaction that maintains a prolonged state

of non-equilibrium leading to macroscopic temporal oscillations and spatial pattern formation that is very life-like.

2.1.1 Belousov-Zhabotinsky reaction

The simplified mechanism for the Belousov-Zhabotinsky reaction is as follows (see [PL68] and [Str94]):

$$Ce(III) \rightarrow Ce(IV) \tag{2.1.1}$$

$$Ce(IV) + CHBr(COOH)_2 \rightarrow Ce(III) + Br^- + other\,products \tag{2.1.2}$$

Equation (2.1.1) is autocatalyzed by BrO_3^-, and strongly inhibited by Br^- ions. Therefore, as $Ce(IV)$ is produced in equation (2.1.1), the rate of equation (2.1.2) increases. This results in a high concentrations of Br^- which inhibits and slows equation (2.1.1). After the discovery of oscillating chemical reactions, in 1968 Prigogine proposed a virtual oscillating chemical reaction system – the Brusselator model.

The net reaction is $\mathcal{A}+\mathcal{B} \rightarrow \mathcal{D}+\mathcal{E}$ with transient appearance of intermediates $\mathcal{X}$ and $\mathcal{Y}$. Here $\mathcal{A}$ and $\mathcal{B}$ are reactants and $\mathcal{D}$ and $\mathcal{E}$ are products. The reaction consists of four steps shown on Table 2.1. Step 3 is autocatalystic, since two $\mathcal{X}$ molecules make three $\mathcal{X}$ molecules and it also has an inhibiting factor because, while $\mathcal{Y}$ is necessary to make the reaction, in this process $\mathcal{Y}$ is also used. Indeed, it is the autocatalystic reaction that causes the chemical oscillations in the Brusselator model. On the basis of the Brusselator model, one can create a realistic oscillating chemical reaction model using the Belousov-Zhabotinsky reaction.

To find the equations that govern the Brusselator model denote by A, B, D and E are the concentrations of $\mathcal{A}$, $\mathcal{B}$, $\mathcal{D}$ and $\mathcal{E}$, respectively.

Assuming that the concentration A and B are held constant during the chemical reaction and that the system has only one spatial dimension, one obtains the following system of differential equations by using the column of the step contribution in the Table 2.1 with proper values of coefficients k_i, $i = 1, 2, 3, 4$, as follows:

$$\begin{aligned} \frac{\partial u_1}{\partial t} &= A - (B+1)u_1 + u_1^2 u_2 + \kappa_1 \frac{\partial^2 u_1}{\partial x^2}, \\ \frac{\partial u_2}{\partial t} &= Bu_1 - u_1^2 u_2 + \kappa_2 \frac{\partial^2 u_2}{\partial x^2}, \end{aligned} \tag{2.1.3}$$

where κ_i ,$i = 1, 2$ are diffusion constants, x is the spatial coordinate and u_i, $i = 1, 2$ are functions of x and t.

Step	Reaction	Step Contribution
1	$\mathcal{A} \rightarrow \mathcal{X}$	$\frac{\partial A}{\partial t} = -k_1 A$ $\frac{\partial u_1}{\partial t} = k_1 A$
2	$\mathcal{B} + \mathcal{X} \rightarrow \mathcal{Y} + \mathcal{D}$	$\frac{\partial B}{\partial t} = -k_2 B u_1$ $\frac{\partial u_1}{\partial t} = -k_2 B u_1$ $\frac{\partial u_2}{\partial t} = k_2 B u_1$ $\frac{\partial D}{\partial t} = k_2 B u_1$
3	$2\mathcal{X} + \mathcal{Y} \rightarrow 3\mathcal{X}$	$\frac{\partial u_1}{\partial t} = -k_3 u_1^2 u_2$ $\frac{\partial u_1}{\partial t} = k_3 u_1^2 u_2$
4	$\mathcal{X} \rightarrow \mathcal{E}$	$\frac{\partial u_1}{\partial t} = -k_4 u_1$ $\frac{\partial E}{\partial t} = k_4 u_1$

Table 2.1: **Reaction Diagram in the Brusselator model.**

We study the dynamics of the local map f, mainly describing trajectories that escape to infinity as well as trajectories that remain bounded. The latter form a Cantor-like set in the plane (of apparently positive area) that is the Julia set of the system. In this chapter we establish existence of this set and describe a procedure that allows one to construct it. Additionally, we discuss the topological structure of the Julia set.

2.1.2 A Coupled Map Lattice Associated with the Brusselator Model

In Section 1.2, we presented how to discretize reaction-diffusion equations to obtain CMLs. By plugging the time discretization (1.2.2) and the space discretizations (1.2.3) into the system (2.1.3), we obtain a coupled map lattice (CML) of the type:

$$u_j(n+1) = f(u_j(n)) + \epsilon g_j(\{u_i(n)\}_{|i-j|\leq s}),$$

where $n \in \mathbb{Z}$ is the discrete time coordinate and j the discrete space coordinate (see [PY04]). Furthermore, $f : \mathbb{R}^2 \to \mathbb{R}^2$ is the *local map* for the CML and is given by

$$f(u_1, u_2) = (a + (1 - \gamma - b)u_1 + \gamma u_1^2 u_2,\ u_2 + bu_1 - \gamma u_1^2 u_2), \tag{2.1.4}$$

where $a = A\Delta t > 0$, $b = B\Delta t > 0$ are two leading parameters, and $\gamma = \Delta t > 0$ is a parameter.

2.2 Linear Analysis

For convenience, we write $f(u_1, u_2) = (f_1(u_1, u_2), f_2(u_1, u_2))$ where

$$\begin{aligned} f_1(u_1, u_2) &= a + (1 - \gamma - b)u_1 + \gamma u_1^2 u_2, \\ f_2(u_1, u_2) &= u_2 + bu_1 - \gamma u_1^2 u_2. \end{aligned}$$

For all values of the parameters $a > 0$, $b > 0$, and $\gamma > 0$ the map f has only one fixed point

$$(v_1, v_2) = (\frac{a}{\gamma}, \frac{b}{a}). \tag{2.2.1}$$

We describe stability of the fixed point. The Jacobian matrix is

$$Jac|_{(v_1,v_2)} = \begin{bmatrix} 1 - \gamma + b & \frac{a^2}{\gamma} \\ -b & 1 - \frac{a^2}{\gamma} \end{bmatrix} \tag{2.2.2}$$

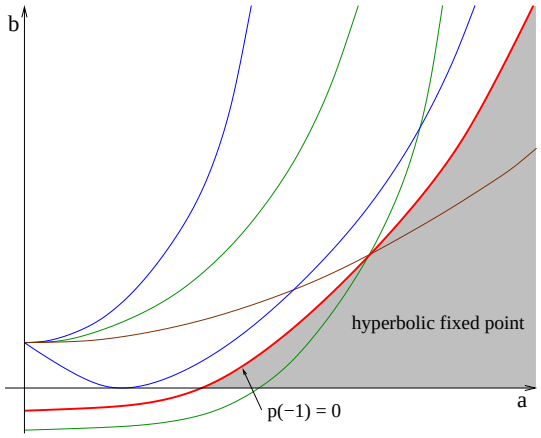

Figure 2.1: When $0 < \gamma < 2$, for any parameters $a > 0$ and $b > 0$ in the shaded region, the local map f has a hyperbolic fixed point. The thick curve represents the graph of $p(-1) = 0$ and is a parabola.

and the characteristic polynomial $p(\lambda)$

$$p(\lambda) = \lambda^2 - (2 - \gamma + b - \frac{a^2}{\gamma})\lambda + (1 - \frac{a^2}{\gamma} - \gamma + a^2 + b). \tag{2.2.3}$$

The discriminant D of $p(\lambda)$ is

$$D = (\gamma - b)^2 + a^2(\frac{a^2}{\gamma^2} - 2 - \frac{2b}{\gamma})$$

and the symmetric axis

$$\lambda_s = \frac{1}{2}(2 - \gamma + b - \frac{a^2}{\gamma}).$$

Note that $p(1) = a^2 > 0$.

CASE 1. **The fixed point is hyperbolic.**

If $p(-1)$ is negative then, by the intermediate value theorem, there exist two eigenvalues λ_1, λ_2 such that one of them, say λ_1, is between -1 and 1, and the other, λ_2, is less than -1 . Therefore, the fixed point is hyperbolic if

$$p(-1) = (1 - \frac{2}{\gamma})a^2 + 2b + 4 - 2\gamma < 0.$$

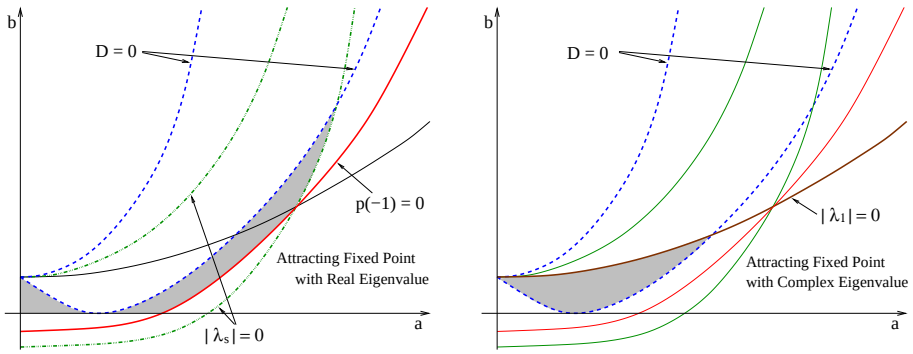

(a) Real Eigenvalues (b) Complex Eigenvalues

Figure 2.2: When $0 < \gamma < 2$, for any parameters $a > 0$, $b > 0$ in the shaded region in (a), the local map f has an attracting fixed point and its Jacobian matrix has real eigenvalues. For those in (b), f also has an attracting fixed point but its Jacobian matrix has complex eigenvalues.

Obviously, the eigenvalues of the characteristic equation $p(\lambda)$ at the hyperbolic fixed point are real numbers.

CASE 2. **The fixed point is attracting.**
The fixed point is attracting if one of the following sets of conditions holds. The first one corresponds to real eigenvalues $\lambda_1 \geq \lambda_2$

$$D = (\gamma - b)^2 + a^2(\frac{a^2}{\gamma^2} - 2 - \frac{2b}{\gamma}) > 0,$$
$$p(-1) = 7(1 - \frac{2}{\gamma})a^2 + 2b + 4 - 2\gamma > 0,$$
$$|\lambda_s| = \left|\frac{1}{2}(2 - \gamma + b - \frac{a^2}{\gamma})\right| < 1,$$

and the second one to complex eigenvalues $|\lambda_1| = |\lambda_2|$

$$D = (\gamma - b)^2 + a^2(\frac{a^2}{\gamma^2} - 2 - \frac{2b}{\gamma}) < 0,$$
$$|\lambda_1| = (1 - \frac{a^2}{\gamma} - \gamma + a^2 + b) < 1.$$

CASE 3. **The fixed point is repelling.**
Similarly, the fixed point is repelling if one of the following sets of conditions

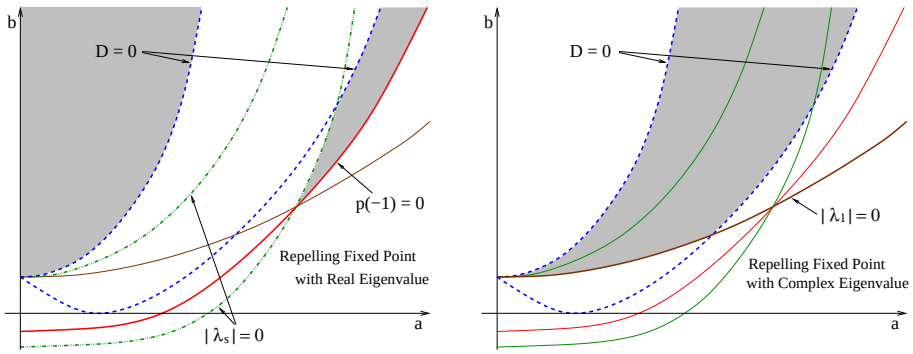

(a) Real Eigenvalues (b) Complex Eigenvalues

Figure 2.3: When $0 < \gamma < 2$, for any parameters $a > 0$, $b > 0$ in the shaded region in (a), the local map f has a repelling fixed point and its Jacobian matrix has real eigenvalues. For those in (b), f also has a repelling fixed point but its Jacobian matrix has complex eigenvalues.

holds. The first one corresponds to real eigenvalues $\lambda_1 \geq \lambda_2$

$$D = (\gamma - b)^2 + a^2(\frac{a^2}{\gamma^2} - 2 - \frac{2b}{\gamma}) > 0,$$
$$p(-1) = (1 - \frac{2}{\gamma})a^2 + 2b + 4 - 2\gamma > 0,$$
$$|\lambda_s| = \left|\frac{1}{2}(2 - \gamma + b - \frac{a^2}{\gamma})\right| > 1,$$

and the second one to complex eigenvalues $|\lambda_1| = |\lambda_2|$

$$D = (\gamma - b)^2 + a^2(\frac{a^2}{\gamma^2} - 2 - \frac{2b}{\gamma}) < 0,$$
$$|\lambda_1| = (1 - \frac{a^2}{\gamma} - \gamma + a^2 + b) > 1.$$

2.3 Escape to Infinity

In this section, we describe a region R in the u_1u_2-plane such that any trajectory in R escapes to infinity, i.e., $|f^n(u_1, u_2)| \to \infty$ as $n \to \infty$. In addition, we check the behavior of these trajectories in this region.

Lemma 2.3.1. For all values of parameters $a > 0$, $b > 0$, and $\gamma > 0$, there exists a region A, that is symmetric with respect to the origin, such that for any point $(u_1, u_2) \in A$,

$$|f_1(u_1, u_2)| > |u_1| + 2a. \tag{2.3.1}$$

Proof. Set $m := \max(|2-\gamma-b|, \gamma+b)$ and define the region A on the plane as follows:

$$A = \{(u_1, u_2) : \gamma u_1^2 |u_2| - m|u_1| - a \geq 0\}.$$

Fix $t > 0$. The following four points lie on the boundary of A in each quadrant:

$$\begin{aligned}
(p_{11}, p_{12}) &:= (t, \frac{mt+a}{\gamma t^2}),\\
(p_{21}, p_{22}) &:= (-t, \frac{mt+a}{\gamma t^2}),\\
(p_{31}, p_{32}) &:= (-t, -\frac{mt+a}{\gamma t^2}),\\
(p_{41}, p_{42}) &:= (t, -\frac{mt+a}{\gamma t^2}).
\end{aligned}$$

It is easy to verify that

$$\begin{aligned}
f_1(p_{11}, p_{12})) > 0, \quad f_1(p_{21}, p_{22}) > 0,\\
f_1(p_{31}, p_{32})) < 0, \quad f_1(p_{41}, p_{42}) < 0.
\end{aligned}$$

We also have that for any $(u_1, u_2) \in \mathbb{R}^2$,

$$\frac{\partial f_1}{\partial u_2}(u_1, u_2) = \gamma u_1^2 \geq 0.$$

It follows that

$$f_1(u_1, u_2) > 0 \text{ for any } u_1 \geq p_{11}, u_2 \geq p_{12} \text{ and } u_1 \leq p_{21}, u_2 \geq p_{22},$$

$$f_1(u_1, u_2) < 0 \text{ for any } u_1 \leq p_{31}, u_2 \leq p_{32} \text{ and } u_1 \geq p_{41}, u_2 \leq p_{42}.$$

In the case $u_1 \geq p_{11}$ and $u_2 \geq p_{12}$ this yields

$$\begin{aligned}
g_1(u_1, u_2) = |f_1(u_1, u_2)| - |u_1| &= a + (1-\gamma-b)u_1 + \gamma u_1^2 u_2 - u_1\\
&= a - (\gamma+b)u_1 + \gamma u_1^2 u_2.
\end{aligned}$$

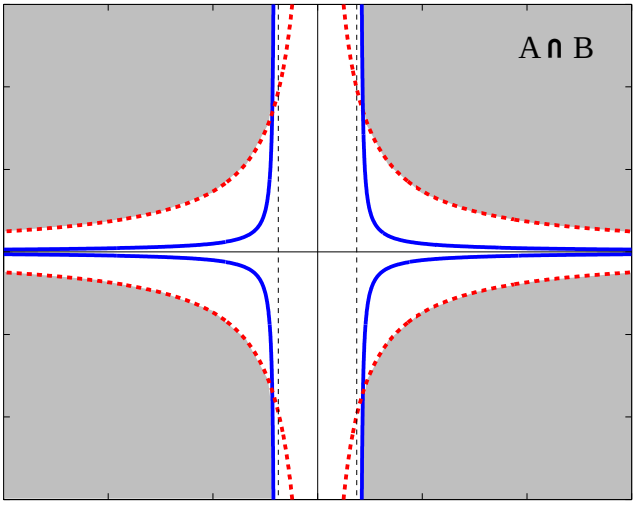

Figure 2.4: The shaded area is the intersection $A \cap B$. The solid line is the boundary of B and has two vertical asymptotic lines, $u_1 = -\sqrt{\frac{2}{\gamma}}$ and $u_1 = \sqrt{\frac{2}{\gamma}}$. The dotted line is the boundary of A.

It is easy to see that

$$g_1(p_{11}, p_{12}) = 2a + t(m - \gamma + b) > 2a$$

and that

$$\frac{\partial g_1}{\partial u_2}(u_1, u_2) = \gamma u_1^2 \geq 0.$$

Thus, in this case (2.3.1) holds. Similar calculations show that (2.3.1) is satisfied in the remaining cases when 1) $u_1 \leq p_{21}$ and $u_2 \geq p_{22}$, 2) $u_1 \leq p_{31}$ and $u_2 \leq p_{32}$, 3) $u_1 \geq p_{41}$ and $u_2 \leq p_{42}$. □

Lemma 2.3.1 does not guarantee that for all $n \geq 2$,

$$|f_1(f^{n-1}(u_1, u_2))| > |f_1(f^{n-2}(u_1, u_2))|.$$

Therefore, we introduce another symmetric region B of the plane and so that $R = A \cap B$.

Lemma 2.3.2. For all values of parameters $a > 0$, $b > 0$, and $\gamma > 0$, there exists a region B, that is symmetric with respect to the origin, such that for any point $(u_1, u_2) \in B$,

$$|f_2(u_1, u_2)| > |u_2|. \tag{2.3.2}$$

Proof. Define the region B as follows:

$$B = \{(u_1, u_2) : |(\gamma u_1^2 - 2)u_2| - b|u_1| \geq 0, \ \ \gamma u_1^2 \geq 2\}.$$

Let $s > \sqrt{\frac{2}{\gamma}}$. Then the following four points lie on the boundary of B in each quadrant:

$$\begin{aligned}
(q_{11}, q_{12}) &:= (s, \frac{bs}{\gamma s^2 - 2}), \\
(q_{21}, q_{22}) &:= (-s, \frac{bs}{\gamma s^2 - 2}), \\
(q_{31}, q_{32}) &:= (-s, -\frac{bs}{\gamma s^2 - 2}), \\
(q_{41}, q_{42}) &:= (s, -\frac{bs}{\gamma s^2 - 2}).
\end{aligned}$$

It is easy to verify that

$$\begin{aligned}
f_2(q_{11}, q_{12})) < 0, \quad f_2(q_{21}, q_{22}) < 0, \\
f_2(q_{31}, q_{32})) > 0, \quad f_2(q_{41}, q_{42}) > 0.
\end{aligned}$$

We also have that for any $(u_1, u_2) \in \mathbb{R}^2$,

$$\frac{\partial f_2}{\partial u_2}(u_1, u_2) = 1 - \gamma u_1^2 < 0$$

since we require that $|u_1| > \sqrt{\frac{2}{\gamma}}$. It follows that

$$f_2(u_1, u_2) < 0 \text{ for any } u_1 \geq q_{11}, u_2 \geq q_{12} \text{ and } u_1 \leq q_{21}, u_2 \geq q_{22},$$

$$f_2(u_1, u_2) > 0 \text{ for any } u_1 \leq q_{31}, u_2 \leq q_{32} \text{ and } u_1 \geq q_{41}, u_2 \leq q_{42}.$$

In the case $u_1 \geq q_{11}$ and $u_2 \geq q_{12}$ this yields

$$\begin{aligned}
g_2(u_1, u_2) = |f_2(u_1, u_2)| - |u_2| &= -u_2 - bu_1 + \gamma u_1^2 u_2 - u_2 \\
&= -2u_2 - bu_1 + \gamma u_1^2 u_2.
\end{aligned}$$

It is easy to see that

$$g_2(q_{11}, q_{12}) = 0$$

and that

$$\frac{\partial g_2}{\partial u_2}(u_1, u_2) = -2 + \gamma u_1^2 \geq 0$$

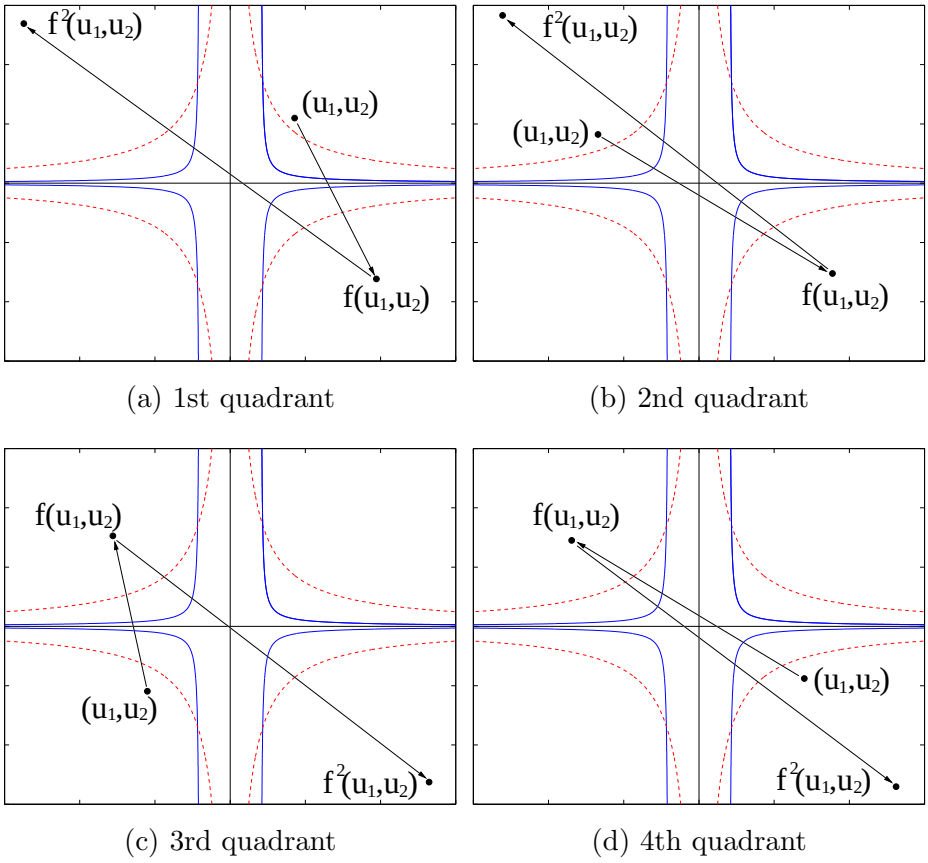

(a) 1st quadrant (b) 2nd quadrant

(c) 3rd quadrant (d) 4th quadrant

Figure 2.5: The way a trajectory escapes to infinity depending on what quadrant it originates in.

due to the requirement that $|u_1| > \sqrt{\frac{2}{\gamma}}$. Thus, in this case (2.3.2) holds. Similar calculations show that (2.3.2) is satisfied in the remaining cases when 1) $u_1 \leq q_{21}$ and $u_2 \geq q_{22}$, 2) $u_1 \leq q_{31}$ and $u_2 \leq q_{32}$, 3) $u_1 \geq q_{41}$ and $u_2 \leq q_{42}$. □

Theorem 2.3.3. For all values of parameters $a > 0$, $b > 0$, and $\gamma > 0$, there exists a forward-invariant region $R = R(a, b, \gamma)$ such that for any point $(u_1, u_2) \in R$, the trajectory $\{f^n(u_1, u_2)\} \subset R$ escapes to infinity.

Proof. We claim that $R = A \cap B$ is the desired region. See Figure 2.4.

Indeed, by construction of the regions A and B we have for any $(u_1, u_2) \in R$,

$$|f(u_1, u_2)| > |(u_1, u_2)|.$$

Figure 2.5 illustrates various routes of escaping to infinity through the region R depending on what quadrant the original point $(u_1, u_2) \in R$ lies in: from the first and the second quadrant the trajectory moves to the fourth quadrant, from the third quadrant and the fourth quadrant it moves to the second quadrant.

By Lemma 2.3.1 (see (2.3.1)), we have that for any $(u_1, u_2) \in R$ with $u_2 > 0$,

$$|f_1(u_1, u_2)| - |u_1| > 2a.$$

In view of Lemma 2.3.2 (see (2.3.2)) this implies that

$$|f(u_1, u_2)| - |(u_1, u_2)| > 2a.$$

Observe that any trajectory $\{f^n(u_1, u_2)\}$ that originates in R visits the second quadrant after at most two iterations and hence, we guarantee that for any $(u_1, u_2) \in R$,

$$|f^2(u_1, u_2)| - |(u_1, u_2)| > 2a.$$

This implies that $|f^n(u_1, u_2)| \to \infty$ as $n \to \infty$. □

In Figure 2.5, one can observe how the trajectories in R escape to infinity. Let R_i be the the partition of R in i^{th}-quadrant in the plane $\mathbb{R}^2$, for $i = 1, 2, 3, 4$, respectively. Then every trajectory which escapes to infinity enters into R_2 or R_4 after at most one iteration, and then it grows to infinity in visiting R_2 and R_4 alternately. More precisely, from Theorem 2.3.3, we conclude

1. $f(R_1) \subset R_4$, and $f(R_3) \subset R_2$,
2. $f(R_2) \subset R_4$, and $f(R_4) \subset R_2$.

These facts will be used in Section 2.4.2.

2.4 Julia Set and Topological Properties

Our goal in this section is to find the maximal region S so that every point in S escapes to infinity while trajectories of points outside S are bounded.

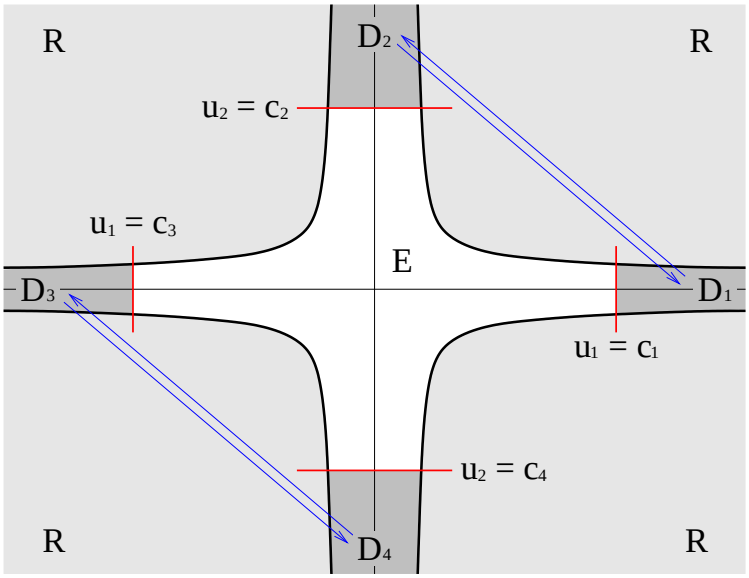

Figure 2.6: D_1 corresponds to D_2 while D_3 corresponds to D_4.

The set $\mathbb{R}^2 \setminus S$ is the Julia set of the system and thus we find various Julia sets corresponding to different values of parameters. We stress that bounded trajectories are the one that are interesting from the physical point of view. We believe that periodic trajectories are dense in the Julia set and that this can be used to justify the existence of oscillating solutions in the Belousov-Zhabotinsky reaction.

2.4.1 Julia Set - Basin of Attraction

In Section 2.3, we found a region R such that every trajectory originated in R escapes to infinity. In this section we prove that for some values of a, b and γ, every trajectory escaping to infinity gets mapped into R after finitely many iterations of f so that the union of all the backward images of R is the desired set S.

Theorem 2.4.1. Assume that $a^2 \leq \gamma$ and $\gamma + b < 1$. Let $\{f^n(u_1, u_2)\}$ be a trajectory that originates in $\mathbb{R}^2 \setminus R$. $\{f^n(u_1, u_2)\}$ is unbounded if and only if there exists a positive integer $m = m(a, b, \gamma, u_1, u_2)$ such that $f^m(u_1, u_2) \in R$. In particular, $\{f^n(u_1, u_2)\}$ escapes to infinity via the region R.

Let c_1, c_2 be sufficiently large positive constants and c_3, c_4 sufficiently large negative constants. Define the following four regions of $\mathbb{R}^2 \setminus R$ (see Figure 2.6):

$$\begin{aligned} D_1 &= \{(u_1, u_2) \notin R : u_1 > c_1\}, \\ D_2 &= \{(u_1, u_2) \notin R : u_2 > c_2\}, \\ D_3 &= \{(u_1, u_2) \notin R : u_1 < c_3\}, \\ D_4 &= \{(u_1, u_2) \notin R : u_2 < c_4\}. \end{aligned}$$

To prove Theorem 2.4.1, we need the following technical lemmas.

Lemma 2.4.2. For any sufficiently large positive c_1, c_2, and negative c_3, c_4, we have

$$f(u_1, u_2) \notin D_3 \cup D_4,$$

for any $(u_1, u_2) \in D_1 \cup D_2$ and

$$f(u_1, u_2) \notin D_1 \cup D_2,$$

for any $(u_1, u_2) \in D_3 \cup D_4$

This statement allows us to study trajectories that originate in $D_1 \cup D_2$ and $D_3 \cup D_4$ separately. We shall consider only trajectories originating in $D_1 \cup D_2$ as the second case is similar.

The following two statements show that any trajectory cannot stay forever in either of the regions D_1 or D_2 and in particular, escape to infinity via these regions.

Lemma 2.4.3. For any sufficiently large $c_1 > 0$ and any $(u_1, u_2) \in D_1$, either $f(u_1, u_2) \notin D_1$ or $f_1(u_1, u_2) < \alpha u_1$ with some $0 < \alpha < 1$.

Lemma 2.4.4. There exists $k \geq 0$ such that for any sufficiently large $c_2 > 0$ and $(u_1, u_2) \in D_2$, the following statements hold:

1. for any $(u_1, u_2) \in D_2$, there exists $m = m(u_1, u_2)$ such that $f^m(u_1, u_2) \notin D_2$;

2. if $n > 0$ is the first time such that $f^n(u_1, u_2) \in D_2$ then $f_2(f^i(u_1, u_2)) \leq u_2 + k$ for all $0 \leq i \leq n - 1$.

The following two statements describe the situation when a trajectory jumps from one of the regions to another.

Lemma 2.4.5. For any sufficiently large $c_1 > 0$ and $c_2 > 0$, and any $(u_1, u_2) \in D_1$, let m_1, m_2 be such that $f^i(u_1, u_2) \in D_1$ for $0 \leq i \leq m_1$, $f^j(u_1, u_2) \in D_2$ for $m_1 < j < m_2$, and $f^{m_2}(u_1, u_2) \in D_1$. Then

$$f_1(f^{m_2-1}(u_1, u_2)) < u_1.$$

Lemma 2.4.6. For any sufficiently large $c_1 > 0$ and $c_2 > 0$, and any $(u_1, u_2) \in D_2$, let m_1, m_2 be such that $f^i(u_1, u_2) \in D_2$ for $0 \leq i \leq m_1$, $f^j(u_1, u_2) \in D_1$ for $m_1 < j < m_2$, and $f^{m_2}(u_1, u_2) \in D_2$. Then

$$f_2(f^{m_2-1}(u_1, u_2)) < u_2 + k,$$

where S is the number in Lemma 2.4.4.

The proofs of these statements can be obtained by carefully examining the behavior of trajectories originated in each of the sets D_i. The desired result on Theorem 2.4.1 is an immediate corollary of Lemmas 2.4.2, 2.4.3, 2.4.4, 2.4.5 and 2.4.6.

Theorem 2.4.1 implies the existence of a Julia set for the local map, and hence, the corresponding evolution operator of the CML also has a Julia set. Theorem 2.4.1 also gives us an explicit way to build the set of all bounded trajectories, the Julia set J of the system:

$$J = \mathbb{R}^2 \setminus \bigcup_{n \geq 0} f^{-n}(R). \tag{2.4.1}$$

The set J is not empty as it contains the fixed point $(v_1, v_2) = (a/\gamma,\, b/a)$ (See Section 2.2). Figure 2.7(a) provides a computer generated image of the Julia set and Figure 2.7(b) shows a magnified piece of the set illustrating its complicated structure. In the next section, we study topological properties of the Julia set.

To generate images of the Julia set for a sufficiently large $N > 0$ we generate the set of points (u_1, u_2) for which

$$f^n(u_1, u_2) \in \mathbb{R}^2 \setminus R,$$

for all $n = 0, 1, 2, ..., N$. One can observe that branches of the Julia set are separated by white regions which are preimages of R. Each branch is further split into more branches and this goes on giving a way to a Cantor-like construction whose limit set is the desired set J.

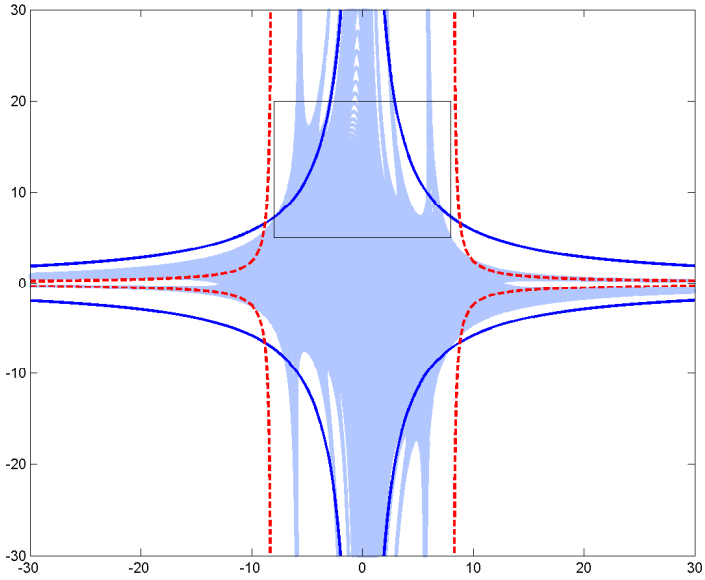

(a)

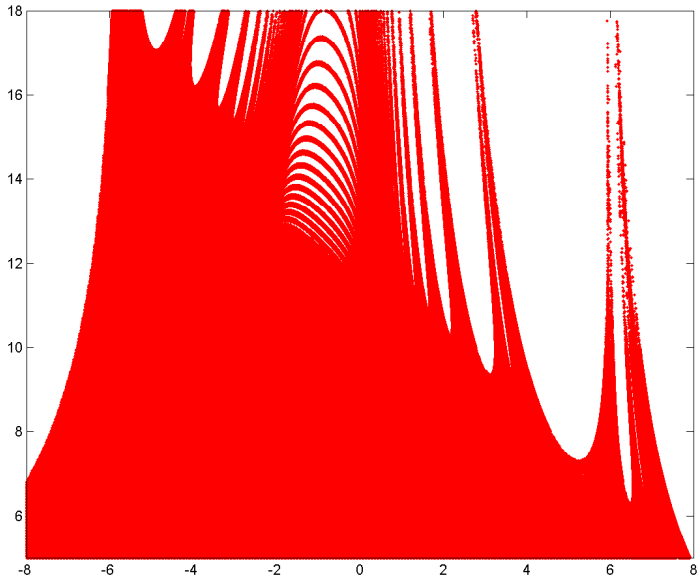

(b)

Figure 2.7: The Julia set of the local map f when the parameter values are $a = 0.07$, $b = 0.245$ and $\gamma = 0.03$. (a) All points in white region escape to infinity. The solid curves represent the boundary of A and the dotted curves represent the boundary of B. (b) Zoom-in region of the rectangle in the Julia set in (a).

2.4.2 Topological Properties

We now discuss topological structure of the Julia set. As seen in Figure 2.7, it is expected that

1. J is closed and unbounded,

2. J has positive area for some parameters.

Additionally, by the definition of the Julia set J, every point on the boundary $\partial(J)$ of J is mapped to another point on $\partial(J)$, while every interior point of J is mapped to another interior point of J. We also believe that J is connected as seen in Figure 2.7.

Theorem 2.4.7. The Julia set J is closed and unbounded.

Proof. We first prove the closedness of the Julia set J. Consider the following two sets S and $\tilde{S}$:

$$S := \bigcup_{n\geq 0} f^{-n}(R) \quad \text{and} \quad \tilde{S} := \bigcup_{n\geq 0} f^{-n}(\text{int}(R)).$$

Clearly, $\tilde{S} \subset S$. So it suffices to show that $S \subset \tilde{S}$. Let $x \in S$. Then $x \in f^{-i}(R)$ for some $i \in \mathbb{N}_0$. This implies that $f^i(x) \in R$ and hence $f^{i+2}(x) \in S$. Thus $x \in \tilde{S}$, and hence, $S = \tilde{S}$. Since $\tilde{S}$ is a union of open sets, $\tilde{S}$ is open and so is S. Therefore, $J = \mathbb{R}^2 \setminus S$ is closed in $\mathbb{R}^2$.

We now show that the Julia set is unbounded. In the proof of Theorem 2.3.3, we saw that $f(R_2) \subset R_4$ and $f(R_4) \subset R_2$. This implies that $R_2 \subset f^{-2i}(R_2) \subset f^{-2(i+1)}(R_2)$ and $R_4 \subset f^{-2j}(R_4) \subset f^{-2(j+1)}(R_4)$ for all $i, j \geq 0$, and hence, there are two sequences $\{A_n\}$ and $\{B_n\}$ of connected sets such that $R_2 \subset A_i \subset f^{-2i}(R_2)$ and $R_4 \subset B_i \subset f^{-2i}(R_4)$. Let $A_\infty = \cup A_i$ and $B_\infty = \cup B_i$. Then by construction, A_∞ and B_∞ are open and disjoint, and their boundaries reach to infinity in $\mathbb{R}^2 \setminus R$. Furthermore, it is easy to show that

$$J = \bigcup_{n=0}^{\infty} f^n \left(A_\infty \cup B_\infty\right).$$

Therefore, the boundary of J also reach to infinity, and hence, J is unbounded. □

On the other hand, for some values of parameters there are bounded trapping region. Clearly, the existence of bounded trapping regions implies that the Julia set J has a positive area.

2.4.3 Julia Set of Traveling Wave Map

In Section 2.3, we found a region $R \subset \mathbb{R}^2$ such that every trajectory in R escapes to infinity and showed that the region R is strictly forward-invariant under the local map f. So, by Theorem 1.5.1, the traveling wave map F_ϵ associated with f also possesses a strictly forward-invariant set $\mathcal{R}$:

$$\mathcal{R} = \otimes_{i=1}^{ls+m} R.$$

Also, in this section, we understood that the Julia set is obtained by using the maximal region of R that is the union of all preimages of R. Therefore, there exists the Julia set $\mathcal{J}_\epsilon$ of the traveling wave map F_ϵ in $(\mathbb{R}^d)^{ls+m}$. The Julia set $\mathcal{J}_\epsilon$ is nonempty since the traveling wave map F_ϵ has a fixed point, which is contained in $\mathcal{J}_\epsilon$. Obviously, the Julia set $\mathcal{J}_\epsilon$ is closed and unbounded, and has a positive volume, too. See [Kan07] and [KP05] for more discussions.

Chapter 3

Dynamics of a Discrete Brusselator Model, Part 2

In this chapter we continue to study the dynamics of the local map focusing on the behavior of bounded trajectories inside the Julia set, while we focused on the behaviors of trajectories which escape to infinity in Chapter 2. In addition, we establish the relationship between the dynamics of the CML and its local map with respect to the evolution operator and the traveling wave map.

Under the same assumption on the parameters as in Theorem 2.4.1, we shall establish existence of

1. an *eventually trapping region* $\tilde{J} \subset J$, i.e., a bounded region in J which every trajectory, originating in J, enters and stays in forever;

2. a *visiting region* $K \subset \tilde{J}$, i.e., a subset of $\tilde{J}$ which every trajectory, originating in J, visits infinitely many times.

Lastly, we present *numerical results* of Julia sets and strange attractors. This will be shown only for certain values of the parameters.

3.1 Eventually Trapping Region

In this section, we deal with the *eventually trapping region*, which is bounded in the plane and contained in the Julia set J. While J is unbounded, the eventually trapping region is bounded. Every trajectory in J enters with a finite number of iteration by the local map f and then stay in the eventually trapping region no matter how large its initial values are.

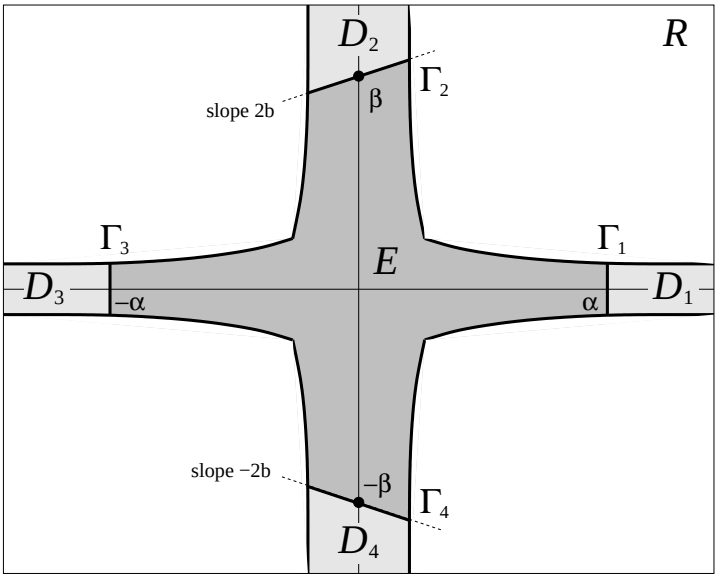

Figure 3.1: Construction of the bounded domain E. E is the shaded region in $\mathbb{R}^2 \setminus R$. $J \cap E$ is the *eventually trapping region*.

3.1.1 Construction and Result

We first construct a bounded domain in the u_1u_2-plane, whose intersection with the Julia set J is the eventually trapping region, as follows.

Let $D := \mathbb{R}^2 \setminus R$ and set two constants

$$\alpha := \frac{2+\sqrt{2}+4b\sqrt{2}}{\gamma a} + \frac{2+2b\sqrt{2}}{\sqrt{\gamma}}, \quad \text{and} \quad \beta := \frac{2+\sqrt{2}+4b\sqrt{2}}{\gamma a},$$

which will be frequently used. We define four subsets in D:

$$\begin{aligned} D_1 &= \{(u_1,u_2) \in D \,|\, u_1 \geq \alpha\} \\ D_2 &= \{(u_1,u_2) \in D \,|\, u_2 \geq 2bu_1 + \beta\} \\ D_3 &= \{(u_1,u_2) \in D \,|\, u_1 \leq -\alpha\} \\ D_4 &= \{(u_1,u_2) \in D \,|\, u_2 \leq -2bu_1 - \beta\}, \end{aligned}$$

and let $E := D \setminus (D_1 \cup D_2 \cup D_3 \cup D_4)$. For convenience, we denote by Γ_i the boundary of E adjacent to D_i for $i = 1, 2, 3, 4$, respectively. Finally, let $\tilde{J} = J \cap E$. See Figure 3.1 for these sets and boundaries.

Theorem 3.1.1. The set $\tilde{J} \subset J$ satisfies:

1. $\tilde{J}$ is bounded and compact;
2. for each $u \in \tilde{J}$, $f(u) \in \tilde{J}$, i.e. $f(\tilde{J}) \subset \tilde{J}$;
3. for each $u \in J$, there exists $n = n(u)$ such that $f^n(u) \in \tilde{J}$.

Theorem 3.1.1 tells us that the set $\tilde{J}$ is a forward-invariant bounded region where all the bounded trajectories of this system, which originate in J, are trapped in $\tilde{J}$ forever once they enter in E. Furthermore, by Theorem 1.5.1, for sufficiently small coupling constant ϵ, the traveling wave map of CML also possesses this eventually trapping region, and hence, so does its evolution operator on the set of traveling wave solutions.

3.1.2 Proof of Theorem 3.1.1

We shall prove $\tilde{J}$ is the eventually trapping region. Since the Julia set J is forward-invariant, it suffices to show that

1. the image $f(E)$ of E under f does not intersect D_i for $i = 1, 2, 3, 4$,
2. for any $u \in \bigcup_{i=1}^{4} D_i \cap J$, there exists $n = n(u) > 0$ such that $f^n(u) \in E$.

Obviously, the set $\tilde{J}$ is bounded and so compact in $\mathbb{R}^2$, since E is compact in $\mathbb{R}^2$. For $k \in \mathbb{R}$, the image of the vertical line $\{u_1 = k\}$ under f is the straight line with slope

$$S_k := -1 + \frac{1}{\gamma k^2}, \tag{3.1.1}$$

which passes through the point P_k on the vertical line $\{u_1 = k\}$

$$P_k := \left(k,\, -\gamma k + a + \frac{\gamma + b}{\gamma k} - \frac{a}{\gamma k^2} \right), \tag{3.1.2}$$

and hence, the equation of the image of the vertical line $\{u_1 = k\}$ is

$$u_2 = \left(-1 + \frac{1}{\gamma k^2} \right) u_1 + (1 - \gamma)k + a - \frac{1 - \gamma - b}{\gamma k} - \frac{a}{\gamma k^2}. \tag{3.1.3}$$

Note that when $k = a/\gamma$, the point P_k in 3.1.2 is the fixed point $P(a/\gamma, b/a)$. One can show that the restriction of f to each vertical line is one-to-one. In particular, we shall use later the fact that the endpoints of each vertical line segment are mapped to the endpoints of the image of the vertical line segment.

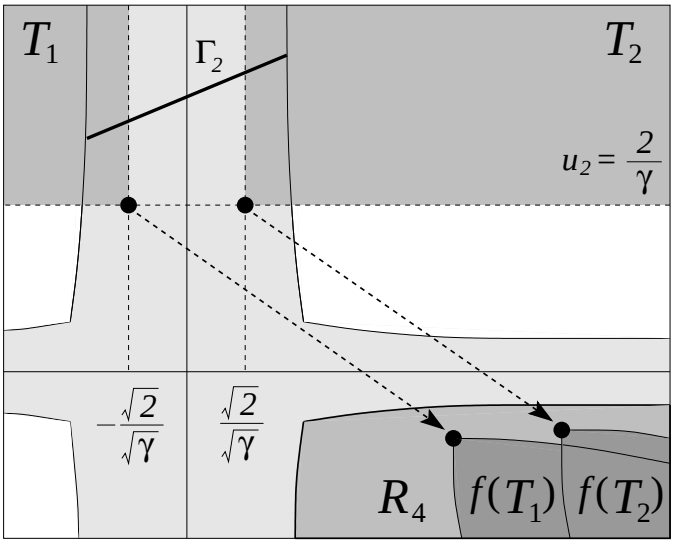

Figure 3.2: The regions T_1 and T_2 and their images under f. $f(T_1) \subset R$ and $f(T_2) \subset R$.

Define two regions T_1 and T_2 in the plane $\mathbb{R}^2$ by

$$T_1 = \{(u_1, u_2) | u_1 \leq -\sqrt{2}/\sqrt{\gamma},\ u_2 \geq 2/\gamma\},$$
$$T_2 = \{(u_1, u_2) | u_1 \geq \sqrt{2}/\sqrt{\gamma},\ u_2 \geq 2/\gamma\},$$

and let R_4 be the intersection of R with the fourth quadrant of $\mathbb{R}^2$

$$R_4 = \{(u_1, u_2) \in R \,|\, u_1 > 0, u_2 < 0\}, \tag{3.1.4}$$

where R is given in Theorem 2.3.3. Then $f(T_1) \in R_4$ and $f(T_2) \in R_4$ because $f(-\sqrt{2}/\sqrt{\gamma},\ 2/\gamma)$ and $f(\sqrt{2}/\sqrt{\gamma},\ 2/\gamma)$ are in R_4 and these points are the left-topmost points in the images $f(T_1)$ and $f(T_2)$, respectively. So we may regard T_1 and T_2 as parts of the escaping region R. See Figure 3.2 to check this extra escaping regions.

We now begin to prove Theorem 3.1.1 with some technical lemmas and their proofs. In the proofs in this section, we shall only consider cases for D_1 and D_2 as those for D_3 and D_4 are similar.

Lemma 3.1.2. Suppose that $(v_1, v_2) \in \mathbb{R}^2 \setminus R$. Then

1. For $v_1 \geq \sqrt{2}/\sqrt{\gamma}$ or $v_2 \geq \sqrt{2}/\sqrt{\gamma}$, $f(v_1, v_2) \notin D_3 \cup D_4$.

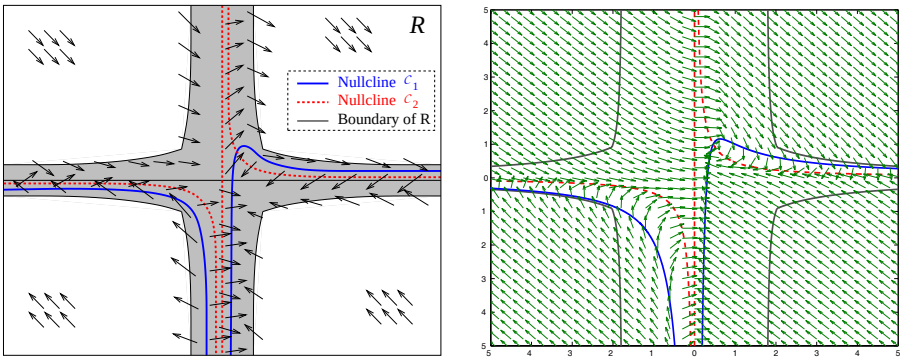

(a) (b)

Figure 3.3: Direction fields of Trajectories. (a) Two nullclines for f_1 and f_2, the solid curves $\mathcal{C}_1$ and the dotted curves $\mathcal{C}_2$, divide the plane into a few regions. Each region has particular direction among the four directions $\nwarrow$, $\nearrow$, $\searrow$ and $\swarrow$. (b) An example of the direction fields of trajectories for the parameter values $a = 0.3$, $b = 0.3$, and $\gamma = 0.65$.

2. For $v_1 \le -\sqrt{2}/\sqrt{\gamma}$ or $v_2 \le -\sqrt{2}/\sqrt{\gamma}$, $f(v_1, v_2) \notin D_1 \cup D_2$.

Proof. If $v_1 \ge \sqrt{2}/\sqrt{\gamma}$ then the image of the vertical line $\{u_1 = v_1\}$ has positive u_1-intercept and u_2-intercept, and its slope S_{v_1} in (3.1.1) is between -1 and $-1/2$. So the image of the vertical line $\{u_1 = v_1\}$ cannot intersect D_3 nor D_4, and hence, $f(v_1, v_2) \notin D_3 \cup D_4$. If $v_2 \ge \sqrt{2}/\sqrt{\gamma}$ then $f_1(v_1, v_2) + f_2(v_1, v_2) = a - \gamma v_1 + v_1 + v_2 > 0$ so that $f(v_1, v_2) \notin D_3 \cup D_4$. Using a similar argument, we can prove the part *2*. □

We denote by $\mathcal{C}_1$ and $\mathcal{C}_2$ two plane curves, which are called *nullclines* for f_1 and f_2, respectively:

$$\mathcal{C}_1 = \{(u_1, u_2) : f_1(u_1, u_2) - u_1 = a - (\gamma + b)u_1 + \gamma u_1^2 u_2 = 0\},$$
$$\mathcal{C}_2 = \{(u_1, u_2) : f_2(u_1, u_2) - u_2 = bu_1 - \gamma u_1^2 u_2 = 0\}.$$

It is obvious that any point on $\mathcal{C}_1$ moves vertically to its image and similarly any point on $\mathcal{C}_2$ moves horizontally. Furthermore, we can assign to every point in each region divided by $\mathcal{C}_1$ and $\mathcal{C}_2$ a direction of the point to its image among the four particular directions as in Figure 3.3(a).

Lemma 3.1.3. $f(\Gamma_2) \cap D_i = \emptyset$ for $i = 1, 2$. Similarly, $f(\Gamma_4) \cap D_j = \emptyset$ for $j = 3, 4$.

Proof. We first show $f(\Gamma_2) \cap D_2 = \emptyset$. Let (v_1, v_2) be a point on Γ_2. It is easy to show that Γ_2 intersects $\mathcal{C}_2$ twice, but not $\mathcal{C}_1$ at all. Let $p = (p_1, p_2)$ and $q = (q_1, q_2)$ with $p_1 < q_1$ be the two intersections of Γ_2 with $\mathcal{C}_2$. We inspect the direction of (v_1, v_2) to its image $f(v_1, v_2)$.

If $v_1 > q_1$ or $v_1 < p_1$ then the direction of (v_1, v_2) to $f(v_1, v_2)$ goes downward and to the right so that $f(v_1, v_2) \notin D_2$. On the other hand, if $p_1 \le v_1 \le q_1$ then the direction goes upward and to the right. Since the points p and q are on $\mathcal{C}_2$, they move horizontally to their image, i.e., $f_2(p_1, p_2) = p_2$ and $f_2(q_1, q_2) = q_2$. By direct calculations, $f(p_1, p_2)$ is located in the right hand side of the curve $u_2 = b/(\gamma u_1)$ of $\mathcal{C}_2$. Note that f_1 and f_2 on Γ_2 satisfy

$$\frac{\partial}{\partial u_1}(f_1(v_1, v_2)) = 6\gamma b v_1^2 + 2\gamma\beta v_1 + 1 - \gamma - b > 0$$
$$\frac{\partial}{\partial u_1}(f_2(v_1, v_2)) = -6\gamma b v_1^2 - 2\gamma\beta v_1 + 3b > 0,$$

since $v_2 = 2bv_1 + \beta$. Thus, $f(v_1, v_2)$ on Γ_2 is monotone increasing as v_1 increases. Therefore, $f(\Gamma_2) \cap \Gamma_2 = \emptyset$, and hence, $f(\Gamma_2) \cap D_2 = \emptyset$. See Figure 3.4(a).

We now show that $f(\Gamma_2) \cap D_1 = \emptyset$. Let r be the intersection of Γ_2 with the vertical line $\{u_1 = \sqrt{2}/\sqrt{\gamma}\}$, i.e., $r = \left(\sqrt{2}/\sqrt{\gamma}, \beta + 2b\sqrt{2}/\sqrt{\gamma}\right)$. For $(v_1, v_2) \in \Gamma_2$,

$$f_1(v_1, v_2) + f_2(v_1, v_2) - \frac{\sqrt{2}}{\sqrt{\gamma}} - \left(\beta + \frac{2b\sqrt{2}}{\sqrt{\gamma}}\right) < a - \sqrt{2\gamma} < 0,$$

so that $f(v_1, v_2)$ lies below the line with slope -1 through r. By direct calculations the line with slope -1 through r does not intersect D_1, and hence, $f(\Gamma_2) \cap D_1 = \emptyset$. See Figure 3.4(b). □

We are finally ready to prove that $f(\tilde{J}) \subset \tilde{J}$. We divide the bounded domain E by two vertical lines $\{u_1 = -\sqrt{2}/\sqrt{\gamma}\}$ and $\{u_1 = \sqrt{2}/\sqrt{\gamma}\}$ into three subregions:

$$E_1 = \{(u_1, u_2) \in E \,|\, u_1 \ge \sqrt{2}/\sqrt{\gamma}\},$$
$$E_2 = \{(u_1, u_2) \in E \,|\, u_1 \le -\sqrt{2}/\sqrt{\gamma}\},$$
$$E_3 = \{(u_1, u_2) \in E \,|\, -\sqrt{2}/\sqrt{\gamma} \le u_1 \le \sqrt{2}/\sqrt{\gamma}\}.$$

We consider vertical line segments in E_i, $i = 1, 2, 3$, and their images under f to prove the following theorem.

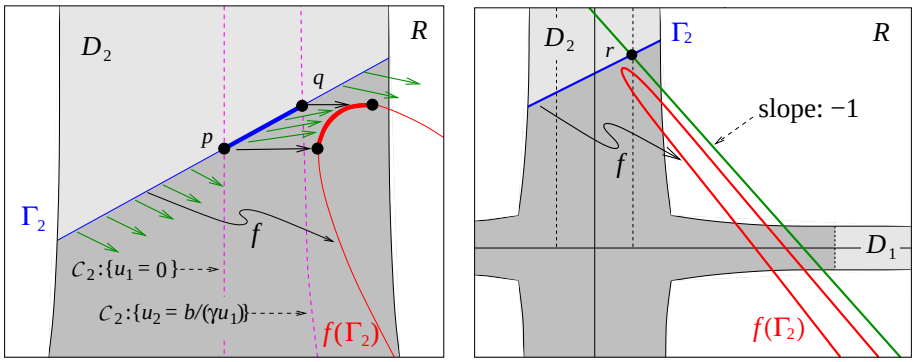

(a) (b)

Figure 3.4: To the proof of Lemma 3.1.3. (a) $f(\Gamma_2) \cap D_2 = \emptyset$. (b) $f(\Gamma_2) \cap D_1 = \emptyset$.

Proposition 3.1.4. $f(E) \cap D_i = \emptyset$ for $i = 1, 2, 3, 4$.

Proof. By Lemma 3.1.2, $f(E_1) \cap D_i = \emptyset$ for $i = 3, 4$. We show that $f(E_1) \cap D_1 = \emptyset$, first. Let $g(x)$ be the u_2-coordinate of the intersection of the vertical line $\{u_1 = \alpha\}$ with the image of a vertical line $\{u_1 = x\}$ passing through E_1:

$$g(x) = \left(-1 + \frac{1}{\gamma x^2}\right)\alpha + (1-\gamma)x + a - \frac{1-\gamma-b}{\gamma x} - \frac{a}{\gamma x^2}.$$

For $\sqrt{2}/\sqrt{\gamma} \le x \le \alpha$, the image of the vertical line $\{u_1 = x\}$ has a negative slope, and

$$g''(x) = \frac{6\alpha - 2(1-\gamma-b)x - 6a}{\gamma x^4} > 0,$$

so that $g(x) \le \max\left(g(\sqrt{2}/\sqrt{\gamma}), g(\alpha)\right)$. Moreover, a simple calculation shows us $\left(\alpha, g(\sqrt{2}/\sqrt{\gamma})\right) \in R_4$ and $(\alpha, g(\alpha)) \in R_4$, where R_4 is given in (3.1.4). Therefore, the intersection $(\alpha, g(x))$ of the vertical line $\{u_1 = \alpha\}$ with the image of the vertical line segment $\{u_1 = x\}$ is in R_4. Thus the image of the vertical line segment $\{u_1 = x\}$ in E_1 does not intersect D_1, and hence, $f(E_1) \cap D_1 = \emptyset$. See Figure 3.5(a).

We show that $f(E_1) \cap D_2 = \emptyset$. Let $h(x)$ be the u_2-coordinate of the intersection of the vertical line $\{u_1 = -\sqrt{2}/\sqrt{\gamma}\}$ with the image of a vertical line $\{u_1 = x\}$ passing through E_1:

$$h(x) = \left(-1 + \frac{1}{\gamma x^2}\right)\left(-\frac{\sqrt{2}}{\sqrt{\gamma}}\right) + (1-\gamma)x + a - \frac{1-\gamma-b}{\gamma x} - \frac{a}{\gamma x^2}. \quad (3.1.5)$$

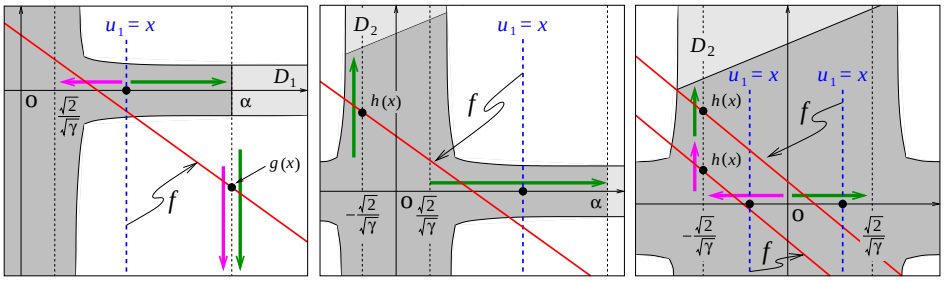

(a) (b) (c)

Figure 3.5: To the proof of Proposition 3.1.4. The dotted lines are the vertical lines and the solid lines are the images of the vertical lines. (a) $f(E_1) \cap D_1 = \emptyset$. (b) $f(E_1) \cap D_2 = \emptyset$. (c) $f(E_3) \cap D_2 = \emptyset$.

For $\sqrt{2}/\sqrt{\gamma} \le x \le \alpha$, $h'(x) > 0$ and also $\left(-\sqrt{2}/\sqrt{\gamma}, h(\alpha)\right) \notin D_2$ by direct calculations. Thus, the intersection $\left(-\sqrt{2}/\sqrt{\gamma}, h(x)\right)$ of the vertical line $\{u_1 = -\sqrt{2}/\sqrt{\gamma}\}$ with the image of the vertical line $\{u_1 = x\}$ is not in D_2 for $\sqrt{2}/\sqrt{\gamma} \le x \le \alpha$, and hence, $f(E_1) \cap D_2 = \emptyset$. See Figure 3.5(b). A similar argument used above for E_1 can be applied to show that $f(E_2) \cap D_i = \emptyset$ for $i = 1, 2, 3, 4$.

We finally show that $f(E_3) \cap D_j = \emptyset$ for $j = 1, 2, 3, 4$. We know that the restriction of f to each vertical line is one-to-one. Also, in Lemma 3.1.3 we already showed that $f(\Gamma_2)$ lies below a line with negative slope which does not intersect D_1. Note that $f(\Gamma_2)$ is composed of the rightmost points of the images of all vertical line segments in E_3, while $f(\Gamma_4)$ is composed of the leftmost points of the images of all vertical line segments in E_3. Thus we have $f(E_3) \cap D_1 = \emptyset$.

For $0 < x \le \sqrt{2}/\sqrt{\gamma}$, $h'(x) > 0$ and $\left(-\sqrt{2}/\sqrt{\gamma}, h(\sqrt{2}/\sqrt{\gamma})\right) \notin D_2$, so that $\left(-\sqrt{2}/\sqrt{\gamma}, h(x)\right) \notin D_2$. On the other hand, for $-\sqrt{2}/\sqrt{\gamma} \le x < 0$, $h'(x) < 0$ and $\left(-\sqrt{2}/\sqrt{\gamma}, h(-\sqrt{2}/\sqrt{\gamma})\right) \notin D_2$, so that $\left(-\sqrt{2}/\sqrt{\gamma}, h(x)\right) \notin D_2$. Thus, the image of any vertical line segment in E_3 does not intersect D_2, and hence, $f(E_3) \cap D_2 = \emptyset$. Similarly, $f(E_3) \cap D_j = \emptyset$ for $j = 3, 4$. See Figure 3.5(c). □

Lemma 3.1.2 allows us to study trajectories that originate in $D_1 \cup D_2$ and $D_3 \cup D_4$ separately. In the following proposition, we shall consider only trajectories originating in $D_1 \cup D_2$ as those originating in $D_3 \cup D_4$ behave similarly.

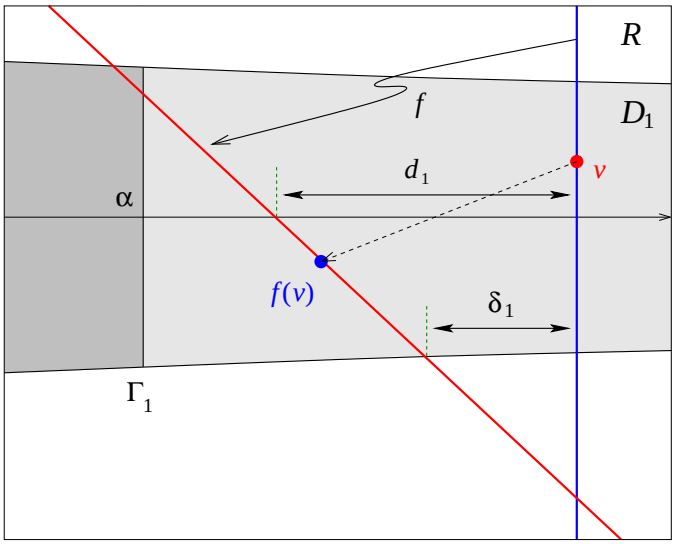

Figure 3.6: Case 1 in Proposition 3.1.5.

Proposition 3.1.5. Let $v = (v_1, v_2) \in \bigcup_{i=1}^{4} D_i \cap J$.

Case 1. If $v \in D_1$ and $f(v) \in D_1$, there exists $\delta_1 > 0$ such that $v_1 - f_1(v) > \delta_1$.

Case 2. If $v \in D_2$ and $f(v) \in D_2$, there exists $\delta_2 > 0$ such that

(a) $f(v)$ lies below the line with slope $2b$ through v,

(b) the distance of $f(v)$ to the line with slope $2b$ through v is larger than δ_2.

Case 3. If $v \in D_1$, $f(v) \in D_2$ and $m > 1$ is the first time such that $f^m(v) \in D_1$, there exists $\delta_3 > 0$ such that $v_1 - f_1(f^{m-1}(v)) > \delta_3$.

Case 4. If $v \in D_2$, $f(v) \in D_1$ and $\tilde{m} > 1$ is the first time such that $f^{\tilde{m}}(v) \in D_2$, there exists $\delta_4 > 0$ such that

(a) $f^{\tilde{m}}(v)$ lies below the line with slope $2b$ through v,

(b) the distance of $f^{\tilde{m}}(v)$ to the line with slope $2b$ through v is larger than δ_4.

Proof. We consider the four cases in order as follows.
Case 1. Consider the image of the vertical line $\{u_1 = v_1\}$. Its slope S_{v_1} in (3.1.1) is negative and its intersection P_{v_1} in (3.1.2) with $\{u_1 = v_1\}$ is

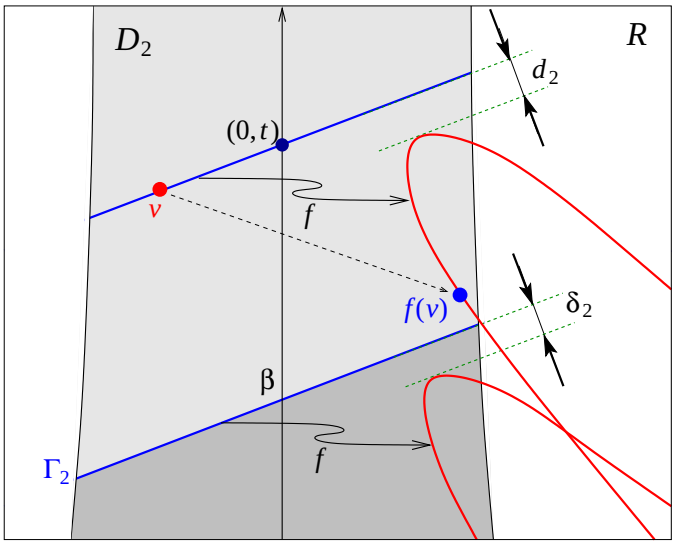

Figure 3.7: Case 2 in Proposition 3.1.5.

located in R_4, and hence, its u_1-intercept is less than v_1. Let $d_1(v_1)$ be the distance of its u_1-intercept point to $\{u_1 = v_1\}$:

$$d_1(v_1) = \gamma v_1 - a - \frac{bv_1}{\gamma v_1^2 - 1}.$$

Then $d_1'(v_1) > 0$. Moreover, as v_1 increases, the slope S_{v_1} decreases to -1 and the boundary of R_4 gets closer to u_1-axis. Thus, the distance $\tilde{d}_1(v_1)$ to $\{u_1 = v_1\}$ from the intersection of its image with the boundary of R_4 also increases as v_1 increases, and hence, the distance $\tilde{d}_1(\alpha)$ at $v_1 = \alpha$ can be chosen as δ_1. See Figure 3.6.

Case 2. In the proof of Lemma 3.1.3, we showed that that $f(\Gamma_2) \cap \Gamma_2 = \emptyset$. Using the same argument, one can prove that the line with slope $2b$ through any point in D_2 does not intersect its image under f. Let $d_2(t)$ be the distance between the line with slope $2b$ through a point $(0,t) \in D_2$ and its image under f:

$$d_2(t) = \inf_{u_1 \in \mathbb{R}} \left(\frac{1}{\sqrt{4b^2+1}} \left| (1+2b)\gamma u_1^2 t - b(1+2b+2\gamma)u_1 + 2ab \right| \right).$$

The expression in the absolute value above is positive for all $t \geq \beta$ and it is linear with respect to t for any fixed $u_1 \in \mathbb{R}$. So $d_2(t)$ increases as t

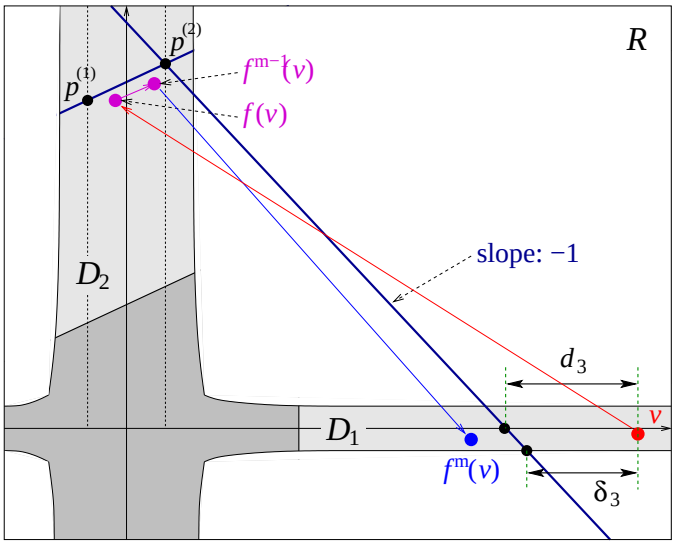

Figure 3.8: Case 3 in Proposition 3.1.5.

increases, and hence, we can take the distance between Γ_2 and $f(\Gamma_2)$ for δ_2. See Figure 3.7.

Case 3. Let $p^{(1)}$ be the intersection of the vertical line $\{u_1 = -\sqrt{2}/\sqrt{\gamma}\}$ with the image of the vertical line $\{u_1 = v_1\}$. By *Case 2*, for all $i = 2, ..., m-1$, $f^i(v)$ lies below the line with slope $2b$ through $p^{(1)}$. Let $p^{(2)}$ be the intersection of the vertical line $\{u_1 = \sqrt{2}/\sqrt{\gamma}\}$ with the line with slope $2b$ through $p^{(1)}$. We use the same argument as in the proof in Lemma 3.1.3 to show that $f^m(v) \in D_1$ lies below the line with slope -1 through $p^{(2)}$. Let $d_3(v_1)$ be the distance of the u_1-intercept point of the line with slope -1 through $p^{(2)}$ to the the vertical line $\{u_1 = v_1\}$:

$$d_3(v_1) = \gamma v_1 - a - \frac{\sqrt{2}}{\sqrt{\gamma}} - \frac{4b\sqrt{2}}{\sqrt{\gamma}} + \frac{1-\gamma-b}{\gamma v_1} + \frac{a}{\gamma v_1^2} + \frac{\sqrt{2}}{\gamma\sqrt{\gamma} v_1^2}.$$

Then $d_3(v_1) > 2/a$ for $v_1 > \alpha$. Note that the boundary of R_4 approaches u_1-axis as u_1 increases. Therefore, the distance of the intersection of the line with slope -1 through $p^{(2)}$ with the boundary of R_4 to the vertical line $\{u_1 = v_1\}$ is proportional to $d_3(v_1)$, and hence, it can be chosen as δ_3. See Figure 3.8.

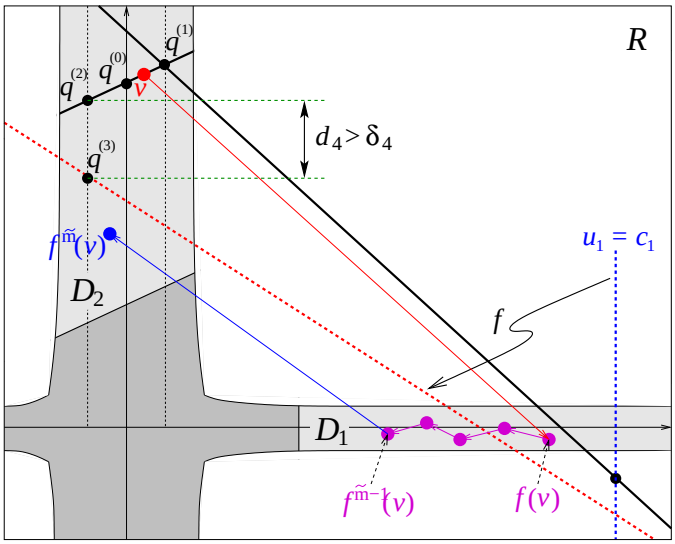

Figure 3.9: Case 4 in Proposition 3.1.5.

Case 4. Let $q^{(0)} := (0, s)$, $q^{(1)}$, and $q^{(2)}$ be the points on the line with slope $2b$ through v at $u_1 = 0$, $u_1 = \sqrt{2}/\sqrt{\gamma}$, and $u_1 = -\sqrt{2}/\sqrt{\gamma}$, respectively. We can use the same argument as in the proof in Lemma 3.1.3 to show that $f(v)$ lies below the line with slope -1 through $q^{(1)}$. Let c_1 be the u_1-coordinate of the line with slope -1 through $q^{(1)}$ at $u_2 = -1/(2\sqrt{\gamma})$. Then it is easy to see that $(c_1, -1/(2\sqrt{\gamma})) \in R_4$. Finally, let $q^{(3)}$ be the point at $u_1 = -\sqrt{2}/\sqrt{\gamma}$ on the image of the vertical line $\{u_1 = c_1\}$.

Let ξ and $\tilde{\xi}$ be the u_2-coordinates of $q^{(2)}$ and $q^{(3)}$, respectively. Let $d_4(s)$ be the distance between $q^{(2)}$ and $q^{(3)}$, i.e., $d_4(s) = |\xi - \tilde{\xi}|$:

$$d_4(s) = \gamma s - \left(\frac{4b\sqrt{2} + \sqrt{2} + 1/2}{\sqrt{\gamma}} + a - 2b\sqrt{2\gamma} \right) + \\ + \frac{1 - \gamma - b}{\sqrt{\gamma}(2b\sqrt{2} + \sqrt{\gamma}s + 1/2)} + \frac{a\sqrt{\gamma} + \sqrt{2}}{\sqrt{\gamma}(2b\sqrt{2} + \sqrt{\gamma}s + 1/2)^2}.$$

It is easy to show $\xi > \tilde{\xi}$. By *Case 1*, $f_1(f^i(v)) < f_1(f^{i-1}(v))$ for $i = 1, ..., \tilde{m} - 2$. Also $h'(x) > 0$ for all $x \geq \alpha$, where $h(x)$ defined in (3.1.5). See Figure 3.5(b). So $f^{\tilde{m}}(v)$ is below the line with slope $2b$ through v.

Simple direct calculations show $d_4'(s) > 0$ and $d_4(\beta) \geq \sqrt{\gamma}/2$, and hence, this number $\sqrt{\gamma}/2$ can be chosen for δ_4. See Figure 3.9. □

Proof of Theorem 3.1.1. By Proposition 3.1.4, $f(\tilde{J}) \subset \tilde{J}$. So this proof is done when we show that all the trajectories originating in $J \setminus \tilde{J}$ enter into $\tilde{J}$.

Assume that there is a trajectory $\{f^i(v_1, v_2) \,|\, (v_1, v_2) \in D_1 \cap J\}$ such that $f^i(v_1, v_2) \in R \setminus E$ for all $i \geq 1$. If $f^k(v_1, v_2) \in D_2 \cap J$ for all $k \geq 1$ then, by *Case 2* in Proposition 3.1.5, the trajectory $\{f^i(v_1, v_2)\}$ would enter into E. Otherwise, i.e., if there is $n_1 > 0$ such that $f^{n_1}(v_1, v_2) \in D_1 \cap J$ then, by either *Case 1* or *Case 3* in Proposition 3.1.5,

$$v_1 - f_1(f^{n_1-1}(v_1, v_2)) \geq \min(\delta_1, \delta_3) > 0,$$

and hence, the trajectory $\{f^i(v_1, v_2)\}$ keeps approaching the boundary Γ_1, and eventually enters into E after a finite number of iterations under f. This is contradictory to our assumption that $f^i(v_1, v_2) \in R \setminus E$ for all $i \geq 1$. Therefore, every trajectory that originates in $D_1 \cap J$ enters into E so that there exists a number $N_1 = N_1(v_1, v_2) > 0$ such that $f^{N_1}(v_1, v_2) \in \tilde{J}$.

On the other hand, suppose that there exists a bounded trajectory in J, $\{f^j(w_1, w_2) \,|\, (w_1, w_2) \in D_2 \cap J\}$ such that $f^j(w_1, w_2) \in R \setminus E$ for all $j \geq 1$. If $f^k(w_1, w_2) \in D_1 \cap J$ for all $k \geq 1$ then, by *Case 1* in Proposition 3.1.5, the trajectory $\{f^n(w_1, w_2)\}$ would enter into E. Otherwise, i.e., if there is $n_2 > 0$ such that $f^{n_2}(w_1, w_2) \in D_2 \cap J$ then, by either *Case 2* or *Case 4* in Proposition 3.1.5,

$$w_1 - f_1(f^{n_2-1}(w_1, w_2)) \geq \min(\delta_2, \delta_4) > 0,$$

and hence, the trajectory $\{f^j(w_1, w_2)\}$ keeps approaching the boundary Γ_2, and eventually enters into E after a finite number of iterations. Similarly, this is contradictory to our assumption, so that there exists a number $N_2 = N_2(w_1, w_2) > 0$ such that $f^{N_2}(w_1, w_2) \in \tilde{J}$.

Using a similar argument above, we can show that for any $(u_1, u_2) \in (D_3 \cup D_4) \cap J$ there exists a $N = N(u_1, u_2)$ such that $f^N(u_1, u_2) \in \tilde{J}$. □

In Theorem 2.4.1 and Theorem 3.1.1, we have two constraints of parameters: $a^2 \leq \gamma$ and $\gamma + b < 1$. These constraints keep us from having any case of hyperbolic fixed points. However, by careful examination, one of the constraints $a^2 \leq \gamma$ can be replaced by $a < 1$ so that we can have some cases of hyperbolic fixed points where the local map f has the Julia set J and the eventually trapping region $\tilde{J}$.

As stated in Section 2.4, the Julia set J is unbounded, so that there exist trajectories in J which begins from infinity. Therefore, every trajectory in J enters in the bounded region $\tilde{J}$ and is trapped inside forever no matter how large its initial values are.

3.2 Visiting Regions

In this section, we discuss so-called the *visiting region* contained in E. In Section 2.4 we understood that the Julia set J is the maximal set of bounded trajectories. We also saw that every bounded trajectory enters in and is trapped in the eventually trapping region $\tilde{J}$. Now we would like to discuss how this trajectory behaves in $\tilde{J}$. We observe that it has some interesting dynamical properties. Every trajectory in $\tilde{J}$ visits some particular region repeatedly and it sometimes forms a strange attractors. In this section we want to discuss these dynamical properties.

3.2.1 Construction and Result

We define a bounded region K in E by

$$K := \{(u_1,\, u_2) \in E \,|\, a/\gamma \le u_1 \le k_1,\, k_2 \le u_2 \le b/(\gamma u_1)\}, \tag{3.2.1}$$

where

$$\begin{aligned} k_1 &= (1+2b)(\sqrt{2}/\sqrt{\gamma})^3 + a/\gamma, \\ k_2 &= \min\left(-1/(2a),\ -\sqrt{2+b}/\sqrt{\gamma},\ (1+b)/a - (\sqrt{\gamma}\sqrt{2+b}/a^2)\right). \end{aligned}$$

Note that the fixed point $P(a/\gamma, b/a)$ is contained in K and it is the left-topmost point of K. See Figure 3.1.

Theorem 3.2.1. Every bounded trajectory $\{f^n(u)\}$ satisfies one of the following two statements:

1. there exists $n_0 = n_0(u) > 0$ such that $f^{n_0}(u) \in K \cap J$,

2. $f^n(u)$ converges to the fixed point $P(a/\gamma,\, b/a) \in K$ as $n \to \infty$.

Theorem 3.2.1 implies that the set $K \cap J$ is the *visiting region*. One can apply Theorem 3.2.1 as follows. Every periodic orbit can be viewed as a bounded trajectory, and it does not converges to the fixed point. So by Theorem 3.2.1, any periodic orbit must visit K periodically, and hence, all the periodic points starts from K. We discuss this application in Section 3.2.3.

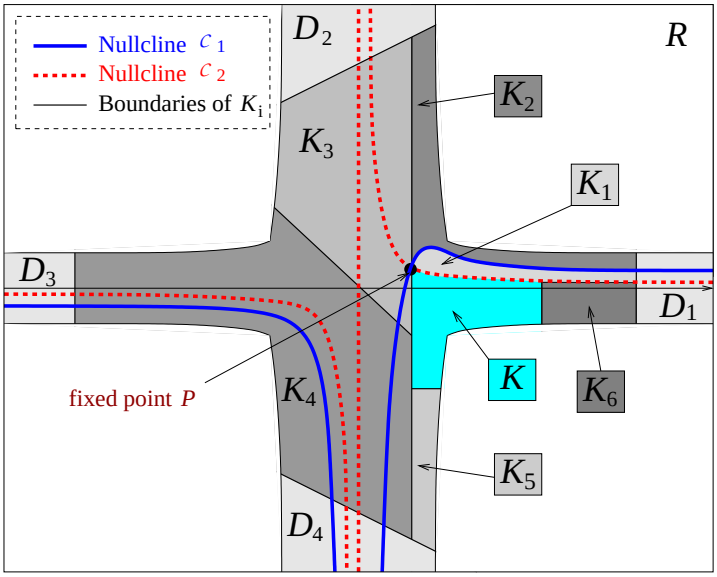

Figure 3.10: The regions K and K_i for $i = 1, 2, 3, 4, 5, 6$. Every bounded trajectory visits K.

3.2.2 Proof of Theorem 3.2.1

We divide the region $E \setminus K$ into the six subregions as follows (See Figure 3.10.):

$$
\begin{aligned}
K_1 &= \{(u_1, u_2) \in E \,|\, u_1 > a/\gamma,\ f_1(u_1, u_2) \le u_1,\ f_2(u_1, u_2) < u_2\},\\
K_2 &= \{(u_1, u_2) \in E \,|\, u_1 \ge a/\gamma,\ f_1(u_1, u_2) > u_1\},\\
K_3 &= \{(u_1, u_2) \in E \,|\, u_1 < a/\gamma,\ u_1 + u_2 \ge 0\},\\
K_4 &= \{(u_1, u_2) \in E \,|\, u_1 < a/\gamma,\ u_1 + u_2 < 0\},\\
K_5 &= \{(u_1, u_2) \in E \,|\, u_1 \ge a/\gamma,\ u_2 < k_2\},\\
K_6 &= \{(u_1, u_2) \in E \,|\, u_1 > k_1,\ f_2(u_1, u_2) \ge u_2\},
\end{aligned}
$$

where k_1 and k_2 are given in (3.2.1). Let $\tilde{K} = K \cup K_6$.

For $(u_1, u_2) \in \mathbb{R}^2$, the distances of (u_1, u_2) and $f(u_1, u_2)$ to the line $\{u_1 + u_2 = 0\}$ are

$$
\frac{|u_1 + u_2|}{\sqrt{2}} \quad \text{and} \quad \frac{|a - \gamma u_1 + u_1 + u_2|}{\sqrt{2}}, \tag{3.2.2}
$$

respectively. When $u_1 + u_2 > 0$, if $u_1 > a/\gamma$ then $f(u_1, u_2)$ approaches the line $\{u_1 + u_2 = 0\}$ or move to the other side of $\{u_1 + u_2 = 0\}$, and if $u_1 < a/\gamma$ then it recedes from $\{u_1 + u_2 = 0\}$. When $u_1 + u_2 < 0$, similarly, if $u_1 < a/\gamma$ then $f(u_1, u_2)$ approaches $\{u_1 + u_2 = 0\}$ or move to the other side of $\{u_1 + u_2 = 0\}$, and if $u_1 > a/\gamma$ then it recedes from $\{u_1 + u_2 = 0\}$. We now consider behaviors of trajectories in J which originate in the subregion K_i for $i = 1, 2, 3, 4, 5, 6$. We first show that every trajectory in $\tilde{J}$ visits $\tilde{K}$, and then in case that the trajectory visits K_6 it visits K later.

Suppose that $(v_1, v_2) \in K_1 \cap J$. Then $f_2(v_1, v_2) < v_2$, i.e., $bv_1 - \gamma v_1^2 v_2 < 0$. So we have

$$f_1(v_1, v_2) = a + (1 - \gamma - b)v_1 + \gamma v_1^2 v_2 > a + (1 - \gamma)v_1 > a/\gamma.$$

Thus, as long as the trajectory $\{f^n(v_1, v_2)\}$ stays in K_1, it converges to the fixed point. Otherwise, when $\{f^n(v_1, v_2)\}$ leaves K_1 it visits $\tilde{K}$ as desired. See the direction field of trajectories in Figure 3.3.

If $(v_1, v_2) \in K_2 \cap J$ then $f_1(v_1, v_2) > v_1$ and $f_2(v_1, v_2) < v_2$, i.e., the direction from (v_1, v_2) to $f(v_1, v_2)$ goes downward and to the right. See Figure 3.3, again. So either the trajectory $\{f(v_1, v_2)\}$ converges to the fixed point, or it visits $\tilde{K} \cup K_1$.

Suppose that $(v_1, v_2) \in K_3 \cap J$. The distance in (3.2.2) of $f^n(v_1, v_2)$ to the line $\{u_1 + u_2 = 0\}$ increases as n increases as long as the trajectory $\{f(v_1, v_2)\}$ stays in K_3. But it is impossible that $f^j(v_1, v_2) \in D_2$ for some $j \in \mathbb{N}$ because the trajectory is already trapped in $\tilde{J}$ by Theorem 3.1.1. So we have either

(1) $f^i(v_1, v_2) \in \tilde{K} \cup K_1 \cup K_2$ for some $i \in \mathbb{N}$, or

(2) $f^n(v_1, v_2) \in K_3$ for all $n \in \mathbb{N}$.

In the case (1), clearly, $\{f^n(v_1, v_2)\}$ satisfies one of the two statements in Theorem 3.2.1. Assume that the case (2) holds. Then $f_1\left(f^{n-1}(v_1, v_2)\right) < a/\gamma$ for all $n \in \mathbb{N}$ so that $\{f^n(v_1, v_2)\}$ recedes from the line $\{u_1 + u_2 = 0\}$ as n increases. But it cannot cross the vertical line $\{u_1 = a/\gamma\}$ nor Γ_2, and thus, it converges to a point on the vertical line $\{u_1 = a/\gamma\}$. Therefore, $f^n(v_1, v_2)$ converges to the fixed point $P(a/\gamma, b/a)$ as $n \to \infty$, since the fixed point for the map f is unique.

Let $(v_1, v_2) \in K_4 \cap J$. Assume that $f^n(v_1, v_2) \in K_4$ for all $n \in \mathbb{N}$. Then $f_1(f^{n-1}(v_1, v_2)) + f_2(f^{n-1}(v_1, v_2)) < 0$ and $f_1(f^{n-1}(v_1, v_2)) < a/\gamma$. So the trajectory $\{f^n(v_1, v_2)\}$ approaches the line $\{u_1 + u_2 = 0\}$ and eventually crosses over it as n increases. But this is contradictory to the assumption.

Thus, either $\{f^n(v_1, v_2)\}$ visits $\tilde{K} \cup K_1 \cup K_2 \cup K_3 \cup K_5$ or converges to the fixed point.

Suppose that $(v_1, v_2) \in K_5 \cap J$. Due to the choice of k_2, $f_1(v_1, v_2) < a/\gamma$ so that $f(v_1, v_2) \in K_4$. If $f^n(v_1, v_2) \in E \setminus K_5$ for all $n \geq 2$ then $\{f(v_1, v_2)\}$ visits $\tilde{K} \cup K_1 \cup K_2 \cup K_3$ as above in the case of $(v_1, v_2) \in K_4 \cap J$. Otherwise, i.e., if $\{f(v_1, v_2)\}$ moves back to K_5, let $m_1 > 0$ be the first time such that $f^{m_1}(v_1, v_2) \in K_5$. We claim that $f^{m_1}(v_1, v_2)$ is closer to the line $\{u_1+u_2 = 0\}$ than (v_1, v_2). When $(v_1, v_2) \in K_5$ is mapped to $f(v_1, v_2) \in K_4$, it recedes from the line $\{u_1+u_2 = 0\}$ with the amount $(|a-\gamma v_1|)/\sqrt{2}$. For $2 \leq n \leq m_1$, $f^n(v_1, v_2)$ approaches $\{u_1+u_2 = 0\}$. When $f(v_1, v_2)$ is mapped to $f^2(v_1, v_2)$, it approaches $\{u_1 + u_2 = 0\}$ with the amount $(|a - \gamma f_1(v_1, v_2)|)/\sqrt{2}$, so that $f^{m_1}(v_1, v_2)$ also approaches $\{u_1 + u_2 = 0\}$ with at least the same amount. It is easy to show that

$$\frac{|a - \gamma v_1|}{\sqrt{2}} \leq \frac{|a - \sqrt{\gamma}\sqrt{2 + b}|}{\sqrt{2}} < \frac{|a - \gamma f_1(v_1, v_2)|}{\sqrt{2}}.$$

Therefore, $f^{m_1}(v_1, v_2)$ is closer to the line $\{u_1 + u_2 = 0\}$ than (v_1, v_2), and hence, either $\{f(v_1, v_2)\}$ visits $\tilde{K} \cup K_1 \cup K_2 \cup K_3$, or it converges to the fixed point.

Let $(v_1, v_2) \in K_6 \cap J$. If $f^n(v_1, v_2) \in E \setminus K_6$ for all $n \geq 1$ then the trajectory $\{f^n(v_1, v_2)\}$ must visit K, by all arguments above. Otherwise, let $m_2 \in \mathbb{N}$ be the first time such that $f^{m_2}(v_1, v_2) \in K_6$. If (v_1, v_2) is mapped into $K_1 \cup K_2 \cup K_6$ then it approaches the line $\{u_1 + u_2 = 0\}$ since $v_1 > a/\gamma$, and hence, $f^{m_2}(v_1, v_2)$ is closer to $\{u_1 + u_2 = 0\}$ than (v_1, v_2). If (v_1, v_2) is mapped into K_3 then it approaches $\{u_1 + u_2 = 0\}$ with the amount $\rho_1 := |a - \gamma v_1|/\sqrt{2}$.

Due to the choice of k_1, $|f_1(v_1, v_2)| < \sqrt{2}/\sqrt{\gamma}$ so that $f^i(v_1, v_2)$ for all $i = 1, 2, ..., m_2$ are below the line

$$\left\{ u_1 + u_2 = \frac{\sqrt{2}}{\sqrt{\gamma}} + \frac{2b\sqrt{2}}{\sqrt{\gamma}} - 2bf_1(v_1, v_2) + f_2(v_1, v_2) \right\}. \tag{3.2.3}$$

When $f(v_1, v_2) \in K_3$ is mapped to $f^{m_2}(v_1, v_2) \in K_6$, it recedes from $\{u_1 + u_2 = 0\}$ with some amount, say, ρ_2. Then ρ_2 is less than the distance of $f(v_1, v_2)$ to the line in (3.2.3), so we have

$$\rho_2 < \left| \frac{1 + 2b}{\sqrt{2}} \left(f_1(v_1, v_2) - \frac{\sqrt{2}}{\sqrt{\gamma}} \right) \right|.$$

Moreover, it is easy to prove the following inequalities:

$$\left|\frac{1+2b}{\sqrt{2}}\left(f_1(v_1,v_2)-\frac{\sqrt{2}}{\sqrt{\gamma}}\right)\right| < \frac{2(1+2b)}{\sqrt{\gamma}} < \frac{|a-\gamma v_1|}{\sqrt{2}} = \rho_1.$$

Therefore, $\rho_1 > \rho_2$ so that $f^{m_2}(v_1, v_2)$ is closer to the line $\{u_1 + u_2 = 0\}$ than (v_1, v_2), and hence, $\{f(v_1, v_2)\}$ visits K.

3.2.3 Applications

In this section, we discuss applications of Theorem 3.2.1. Every periodic orbit can be viewed as a bounded trajectory, so by Theorem 3.2.1 it visits the visiting region $K \cap J$ infinitely many times, periodically.

In order to confirm this fact, we would like to find a periodic orbit of period two. To get this periodic orbit, we simply solve the equations $f^2(u_1, u_2) = (u_1, u_2)$. Then we have four solutions (x_i, y_i), $i = 1, 2, 3, 4$, as follows:

$$x_i = \frac{a}{\gamma} \pm \frac{1}{\gamma}\sqrt{a^2+\gamma-\frac{b\gamma \pm \sqrt{\gamma^2(2-\gamma-b)^2+4\gamma a^2(2-\gamma)^2}}{2-\gamma}},$$
$$y_i = \frac{\gamma b x_i + \gamma^2 x_i - 2\gamma x_i + 2a - \gamma a}{\gamma^2 x_i^2}.$$

One can prove that at least two of the four solutions (x_i, y_i) are real solutions. Therefore, we conclude that for all values of parameters a, b and γ there exist at least two periodic points of period two. Moreover, by Theorem 3.2.1, at least one of the points (x_i, y_i) must be located in the visiting region $K \cap J$.

Additionally, when all the periodic orbits are numerically calculated, it is sufficient that we inspect the visiting region $K \cap J$ only. The detailed discussion of this topic is given in [Kan07].

3.3 Numerical Results

We study in more detail the eventually trapping region $\tilde{J}$. The dynamics inside $\tilde{J}$ depends on the type of the unique fixed point $P(a/\gamma, b/a)$. Rigorous mathematical analysis of this situation is quite difficult and is yet to be carried out.

In this section, we present here some numerical results on local behavior around the fixed point in the Julia set J. We consider three cases when the fixed points are attracting, repelling and hyperbolic.

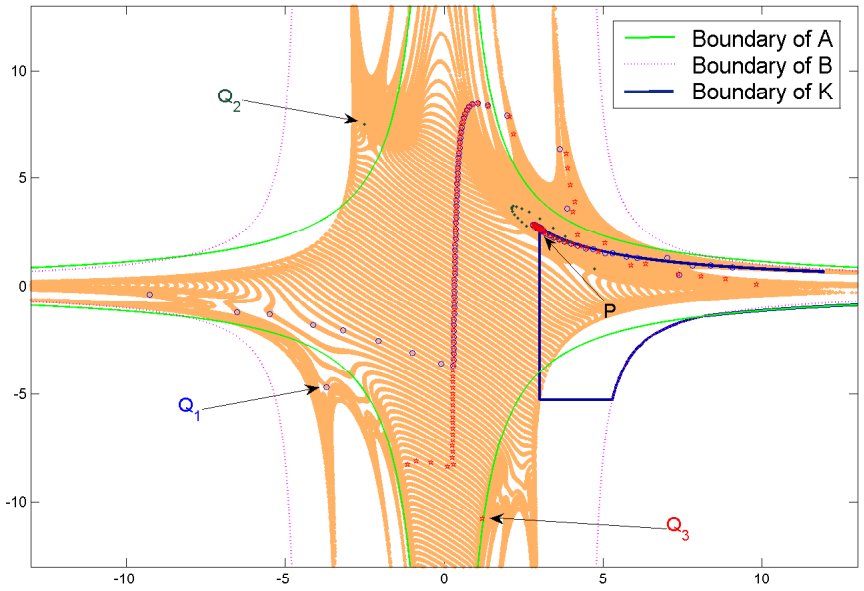

(a)

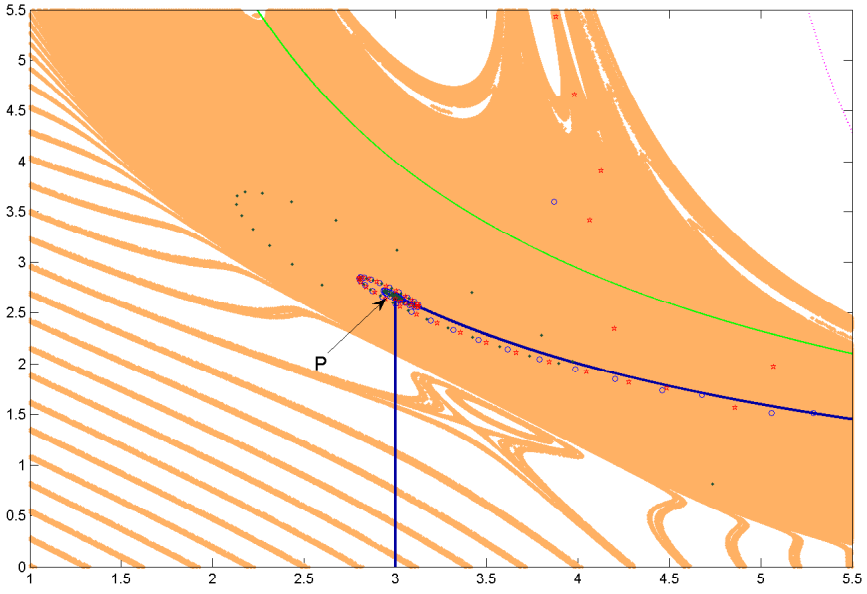

(b)

Figure 3.11: Julia set and bounded trajectories for $a = 0.3$, $b = 0.8$, $\gamma = 0.1$. (a) Shown are the Julia set J, the region K bounded by the thick curves, boundaries for A and B, and the fixed point P. White points escape to infinity while grey points converge to the fixed point. (b) Zoom-in region around the fixed point.

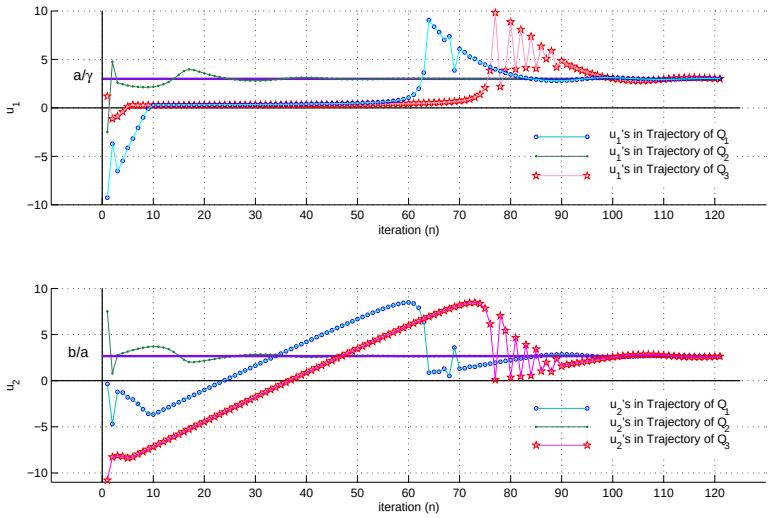

Figure 3.12: Time series with respect to u_1 and u_2 for $a = 0.3$, $b = 0.8$, $\gamma = 0.1$. These three trajectories start at $Q_1 = (-9.265, -0.359)$, $Q_2 = (-2.5, 7.5)$, and $Q_3 = (1.2, -10.79)$, and they eventually attracts to the fixed point $P(3, 8/3)$.

Our numerical study suggests that when the fixed point is

1. attracting all trajectories in J except periodic orbits converge to it;

2. repelling or hyperbolic the map f possesses a strange attractor within the eventually trapping region of extremely complicated topological structures.

The attractors vary widely for different values of the parameters a, b, and γ. The numerical methods used in this section are based on the methods in [ASY96], [Cho05], and [GMBC96].

3.3.1 Attracting Fixed Point: $a = 0.3$, $b = 0.8$, $\gamma = 0.1$

The grey region in Figure 3.11(a) represents the Julia set J. Figure 3.11(b) shows how trajectories converges to the fixed point around it. It is numerically observed that every trajectory that originates in the grey region $\tilde{J}$ converges to the fixed point while all the points in white region escapes to infinity.

We pick three points Q_i in J: $Q_1 = (-9.265, -0.359)$, $Q_2 = (-2.5, 7.5)$, and $Q_3 = (1.2, -10.79)$. Then we iterate these points more than 120 times by f. In Figure 3.12, we observe that all three trajectories originating at these points Q_i converge to the fixed point $P(3, 8/3)$ after about 100 iterations by f. This result strongly supports that every bounded trajectory attracts to the fixed point except periodic orbits no matter how large the initial values of the trajectory are.

One can show that there exists a small bounded trapping region which is connected. This trapping region can be extended to the infinity inside J by taking the union of all backward image of the trapping region. Clearly, this extended trapping region is connected since it contains the fixed point. Therefore, there exist trajectories in J that originate from the sufficiently large initial values.

For these parameters, we have two complex eigenvalues of the Jacobian matrix at the fixed point so that the trajectories in Figure 3.11(b) converge to the fixed point with spiral shape. Numerically computed Lyapunov exponents of the system are both negative, -0.0583.

3.3.2 Repelling fixed points: $a = 0.25$, $b = 0.65$, $\gamma = 0.25$

The grey region in Figure 3.13(a) is the Julia set. The iteration of a point chosen randomly in the Julia set J would produce essentially the same black set in the grey region. The white region consists of initial values whose trajectories escapes to infinity. Figure 3.13(b) shows what the strange attractor looks like. This strange attractor appears around the fixed point $P(1, 2.6)$. In Figure 3.13 we observe that the attractor intersects K. The fixed point, however, the left-topmost point of K, is not contained in the attractor. This is because the fixed point is repelling so that it is impossible to have any trajectory converging to the fixed point.

This is similar to the previous case of the attracting fixed point. The local map also possesses a bounded trapping region in $\tilde{J}$, which is extended to infinity by using the union of all the backward images under f. So there exist bounded trajectories whose initial values are as large as necessary and they are eventually trapped in the bounded trapping region. Once trapped, they exhibit chaotic behaviors in the trapping region as shown in Figure 3.13.

The eigenvalues of the Jacobian matrix at the fixed point are complex numbers. Numerical approximation of the Lyapunov exponents on the attractor yields one positive number 0.0374 and one negative number. The times series of the trajectory originating at $(3, 0.5)$ in Figure 3.14 shows us

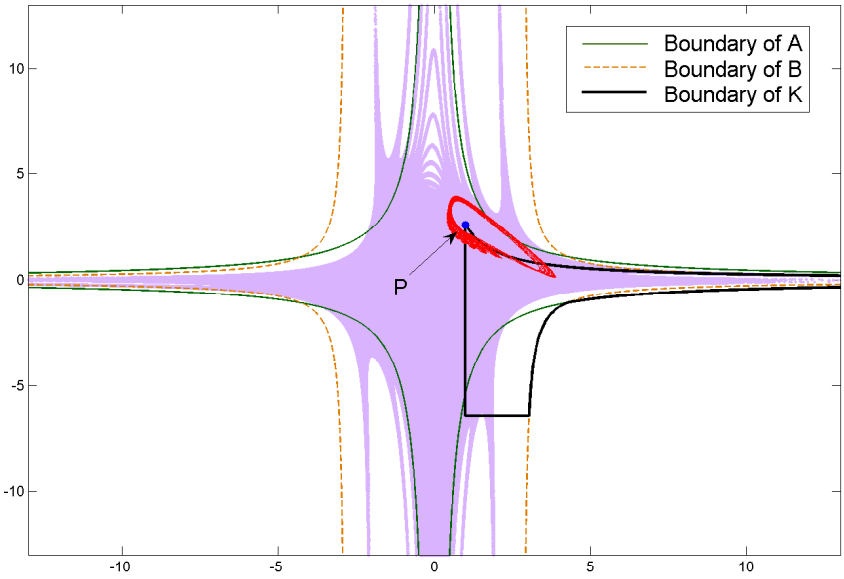

(a)

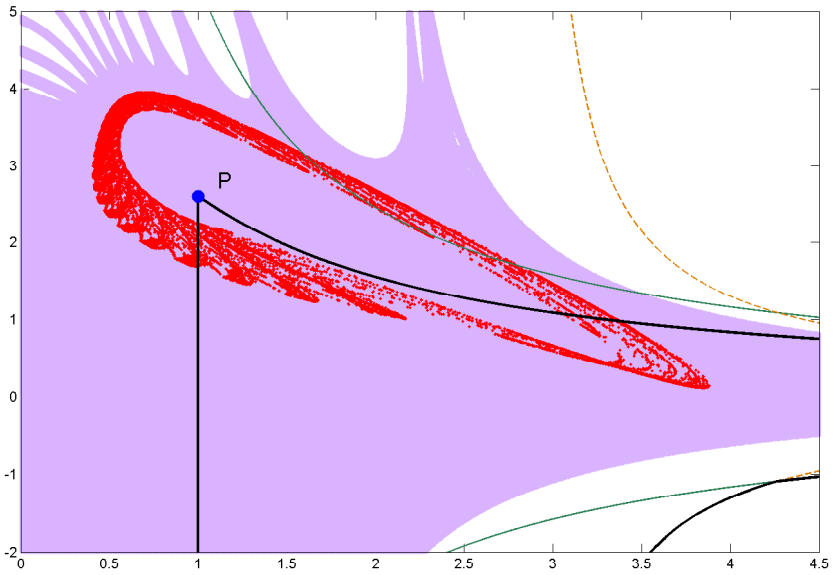

(b)

Figure 3.13: Julia set and strange attractor for $a = 0.25$, $b = 0.65$, $\gamma = 0.25$. (a) Shown are the Julia set J, the region K bounded by the thick curves, boundaries for A and B, and the fixed point $P(1, 2.6)$. (b) Zoom-in region around the fixed point.

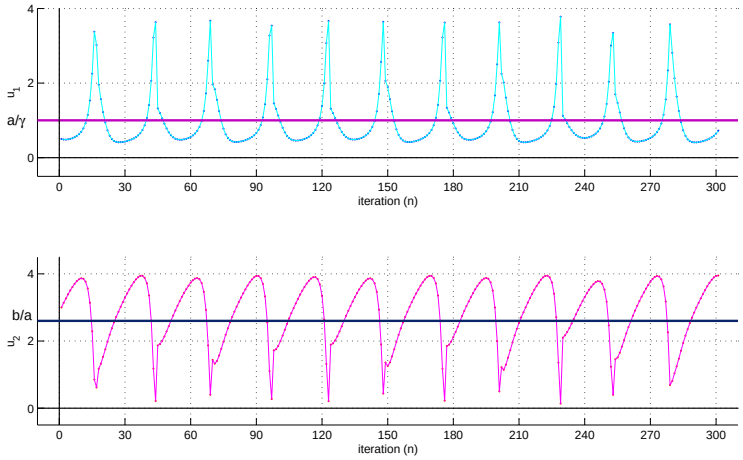

Figure 3.14: Time series with respect to u_1 and u_2 for $a = 0.25$, $b = 0.65$, $\gamma = 0.25$.

how a trajectory behaves in the attractor. The trajectory does not show any convergence nor any periodic behavior in the time series. This means that it displays chaotic behaviors.

3.3.3 Hyperbolic fixed points: $a = 0.8$, $b = 0.2$, $\gamma = 0.25$

In Figure 3.15(b) the strange attractor still appears around the fixed point $P(3.2, 0.25)$. We observe that the attractor intersects K. Also the fixed point, the left-topmost point of K, is contained in the attractor. In the previous case where the fixed point is repelling, the fixed point is not included in the attractor.

Throughout the calculation, the orbit appears to have a positive Lyapunov exponent 0.1793 and it fails to approach periodic behavior. In Figure 3.16 we observe that the time series of a trajectory oscillates around the fixed point but it does not converge to the fixed point. It exhibits chaotic behaviors.

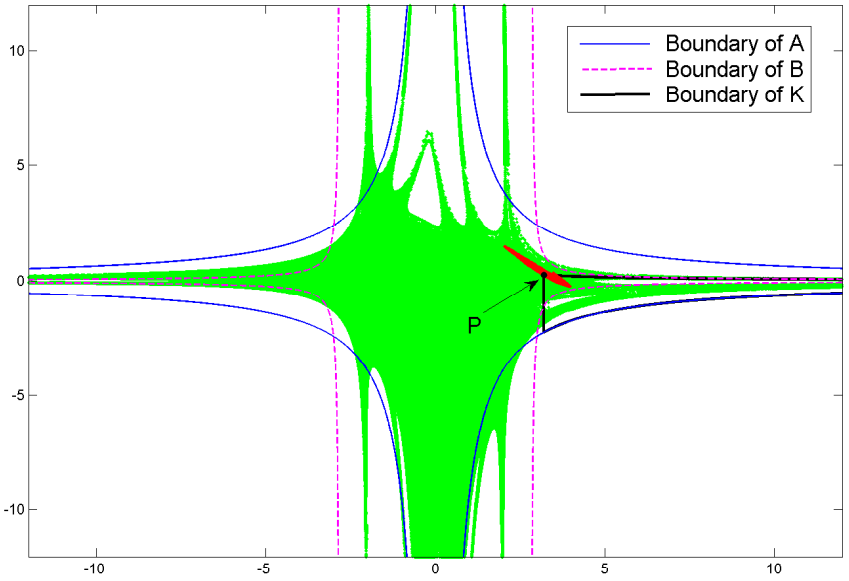

(a)

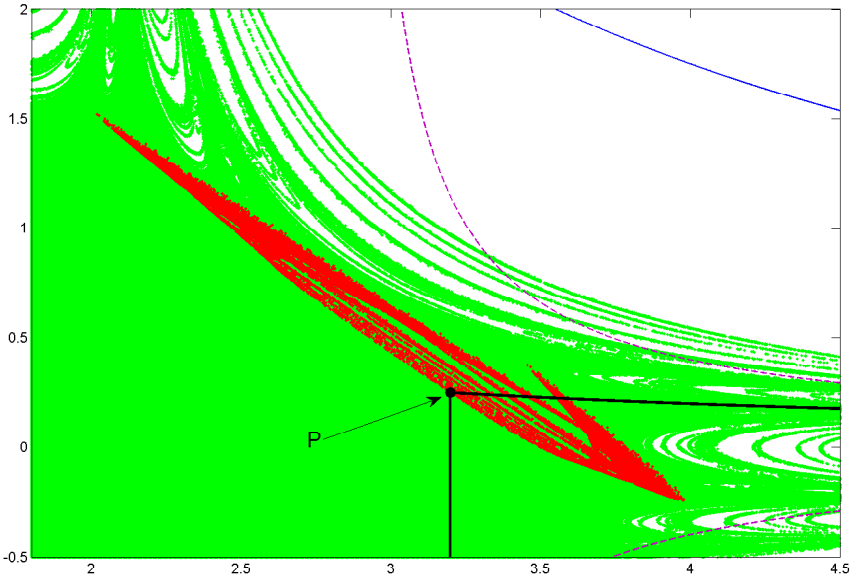

(b)

Figure 3.15: Julia set and attractor for $a = 0.8$, $b = 0.2$, $\gamma = 0.25$. (a) Shown are the Julia set J, the region K bounded by the thick curves, boundaries for A and B, and the fixed point $P(3.2, 0.25)$. (b) Zoom-in region around the fixed point.

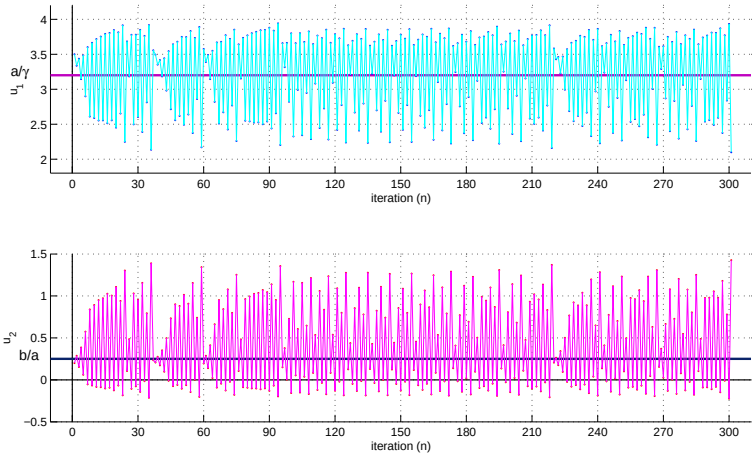

Figure 3.16: Time series with respect to u_1 and u_2 for $a = 0.8$, $b = 0.2$, $\gamma = 0.25$.

References

[AGN94] V. Afraimovich, L. Glebsky, and V. I. Nekorkin, *Stability of stationary states and topological spatial chaos in multidimensional lattice dynamical systems*, Random and Computational Dynamics **2** (1994), 287–305.

[AP93] V. Afraimovich and Ya. Pesin, *Travelling waves in lattice models of multi-dimensional and multi-component media : I. general hyperbolic properties*, Nonlinearity **6** (1993), 429–455.

[ASY96] K. Alligood, T. Sauer, and J. Yorke, *Chaos, an introduction to dynamical systems*, Springer, 1996.

[BK96] J. Bricmont and A. Kupiainen, *High temperature expansions and dynamical systems*, Communications in Mathematical Physics **178** (1996), 703–732.

[BS88] L. Bunimovich and Ya. Sinai, *Space-time chaos in coupled map lattices*, Nonlinearity **1** (1988), 491–516.

[Bun95] L. Bunimovich, *Coupled map lattices: one step forward and two steps back*, Physica D **86** (1995), 248–255.

[Cho05] G. H. Choe, *Computational ergodic theory*, Springer, 2005.

[GMBC96] L. Gardini, C. Mira, A. Barugola, and J. C. Cathala, *Nonlinear dynamics and chaos with applications to physics, biology, chemistry and engineering*, Nonlinear Science, vol. 20, World Scientific Publishing, 1996.

[HH52] A. Hodgkin and A. Huxley, *A quantative description of membrane current and its application to conduction and excitation in nerve*, Journal of Physiology **117** (1952), 501–544.

[JP98] M. Jiang and Ya. Pesin, *Equilibrium measures for coupled map lattices: Existence, uniqueness and finite-dimensional approximations*, Communications in Mathematical Physics **193** (1998), 675–711.

[Kan93] K. Kaneko, *Theory and applications of coupled map lattices*, Wiley, 1993.

[Kan07] H. Kang, *Dynamics of local map of a discrete brusselator model: Eventually trapping regions and strange attractors*, Discrete and Continuous Dynamical System (2007), Accepted for Publication (to appear).

[KK92] G. Keller and M. Kuenzle, *Transfer operators for coupled map lattices*, Ergodic Theory and Dynamical Systems **12** (1992), 297–318.

[KP05] H. Kang and Ya. Pesin, *Dynamics of a discrete brusselator model: Escape to infinity and julia set*, Milan Journal of Mathematics **73** (2005), 1–17.

[KPP37] A. Kolmogorov, I. Petrovskii, and N. Piskunov, *A study of the diffusion equation with increase in the amount of substance, and its application to a biological problem in selected works of a. kolmogorov*, Bullutin of Moscow University, Mathematical Mechanics **1** (1937), 1–26.

[OP99] D. Orendovici and Ya. Pesin, *Chaos in traveling waves of lattice systems of unbounded media*, Proceedings of the IMA Volumes in Mathematics and its Applications **119** (1999), 327–359.

[PL68] I. Prigogine and R. Lefever, *Symmetry-breaking instabilities in dissipative systems*, Journal of Chemical Physics **48** (1968), 1695–1700.

[PS91] Ya. Pesin and Ya. Sinai, *Space-time chaos in chains of weakly interacting hyperbolic mappings*, Advances in Soviet Mathematics **3** (1991), 165–198.

[PY04] Ya. Pesin and A. Yurchenko, *Some physical models of the reaction-diffusion equation and coupled map lattices*, Russian Math. Surveys **8** (2004), 177–218.

[Rob99] C. Robinson, *Dynamical systems : stability, symbolic dynamics, and chaos*, CRC Press, 1999.

[Str94] S. Strogatz, *Nonlinear dynamics and chaos with applications to physics, biology, chemistry and engineering*, Studies in Nonlinearity, Addison-Wesley, 1994.

[Tys76] J. Tyson, *The belousov-zhabotinskii reaction*, Lecture Notes in Biomathematics 10, Addison-Wesley, 1976.

Vita

Hunseok Kang

Born: April 1, 1974, Seoul, KOREA Republic of.

Education

Post-Doc	June 2007 ~	Hokkaido University Mentors: Ichiro Tsuda and Michiko Yuri
PhD	August 2007	The Pennsylvania State University Thesis Advisor: Yakov Pesin
BA	February 1997	Chung-Ang University at Seoul *summa cum laude*

Publications

1. *Dynamics of Local Map of a Discrete Brusselator Model: Eventually Trapping Regions and Strange Attractors.*
   Hunseok Kang. Accepted for publication, May 2007, Discrete and Continuous Dynamical Systems.

2. *Dynamics of a Discrete Version of Brusselator Model: Escapes to Infinity and Julia Set.*
   Hunseok Kang and Yakov Pesin. Milan Journal of Mathematics, October 2005.

3. *Fractal structures of a Turing Model of Morphogenesis.*
   Hunseok Kang. Preprint at Pennstate Univ., 2007.

4. *Dynamics of Local Map for a Discrete Brusselator Model.* PhD dissertation, August 2007.